

MZ-TH/97-28
 MPI/PhT/97-47
 UCSD/97-18
 hep-ph/9707517
 July 1997

Gauge-Independent Analysis of $K_L \rightarrow e\mu$ in Left-Right Models

Zoltan Gagai-Palffy,^a Apostolos Pilaftsis^{b†} and Karl Schilcher^{c‡}

^a*Institut für Physik, THEP, Johannes Gutenberg-Universität, 55099 Mainz, Germany*

^b*Max-Planck-Institut für Physik, Föhringer Ring 6, 80805 Munich, Germany*

^c*Department of Physics, Univ. of California, San Diego, La Jolla, CA 92093-0319, USA*

ABSTRACT

The lepton-flavour-violating decay $K_L \rightarrow e\mu$ is studied in detail within the context of $SU(2)_R \otimes SU(2)_L \otimes U(1)_{(B-L)}$ models, which include heavy Majorana neutrinos. Particular attention is paid to the gauge independence of this decay process to one loop. In analogy with earlier studies on the $K^0 \bar{K}^0$ mixing, it is explicitly shown how restoration of gauge invariance occurs in the decay amplitude containing the box diagrams, when the relevant Higgs-dependent self-energy and vertex graphs are taken into account in the on-shell skeleton renormalization scheme. Based on the analytic expressions so derived, we find that the branching ratio $B(K_L \rightarrow e\mu)$ can be considerably enhanced due to the presence of left- and right-handed currents in the loop, and can reach values close to or even larger than the present experimental limit 3.3×10^{-11} in the manifest left-right symmetric model. Constraints on the parameter space of typical left-right models are derived from the possible decay $K_L \rightarrow e\mu$ and a global analysis of other low-energy data.

[†]e-mail address: pilaftsi@mppmu.mpg.de

[‡]Permanent address: Institut für Physik, THEP, Johannes Gutenberg-Universität, 55099 Mainz, Germany. E-mail address: schilcher@dipmza.physik.uni-mainz.de

1 Introduction

Experiments involving kaons or kaon decays have reached a high level of accuracy and are therefore very sensitive to probe new physics beyond the minimal Standard Model (SM). For example, studying the small mass difference ΔM_K between the long-lived kaon K_L and the short-lived one K_S is one such measurement of amazing precision. In the $K^0\bar{K}^0$ system, the observable $\Delta M_K/M_K$ is very accurately established at the level of 10^{-15} [1], in line with predictions in the SM [2]. Other experiments sensitive to new-physics scenarios look for possible lepton-flavour-violating decays of the type $K_L \rightarrow e\mu$. The experimental upper bound on the branching ratio $B(K_L \rightarrow e\mu)$ is very stringent [1], *i.e.*,

$$B_{\text{exp}}(K_L \rightarrow e\mu) < 3.3 \times 10^{-11}, \quad (1.1)$$

at 90% confidence level. Ongoing experiments at BNL, KEK and, more recently, at DAΦNE are expected to lower the above bound by one order of magnitude. Although the decay $K_L \rightarrow e\mu$ is strictly forbidden in the SM due to the absolute conservation of the individual leptonic quantum numbers, lepton-flavour violation occurs almost inevitably in many of its extensions. For example, many studies have been devoted to analyze such a decay in models based on technicolour [3], supersymmetry [4], horizontal symmetry [5], extended scalar [6] and gauge sector [7,8,9,10]. Thus, experiments on $K_L \rightarrow e\mu$ provide a unique opportunity either to discover new physics or to constrain efficiently the parameter space of these theories.

In this paper, we shall present a careful analysis of $K_L \rightarrow e\mu$ in left-right models, which are realized by the gauge group $SU(2)_R \otimes SU(2)_L \otimes U(1)_{(B-L)}$ and include heavy Majorana neutrinos [11]. These theories also allow for scenarios with high Dirac mass terms of order of top quark mass without invalidating experimental limits on light neutrino masses. In these scenarios, the usual see-saw suppression relations [12] for the light-heavy neutrino mixings may be avoided. In particular, it has been found that the large Dirac masses give rise to a non-decoupling behaviour of the heavy neutrinos in loops [13,14], thereby enhancing significantly the decay rate for possible lepton-flavour-violating processes, such as $Z \rightarrow e\tau$ [15] and the size of related new-physics observables at LEP1 [16,17]. This feature makes the left-right models very attractive. Apart from taking properly into consideration the non-decoupling effect of heavy neutrinos, we shall also analyze the impact of other low-energy data on the theoretical prediction for $B(K_L \rightarrow e\mu)$, such as those coming from the non-observation of the decay $\mu \rightarrow e\gamma$ and the $K_L K_S$ mass difference.

Another important issue, which is to be discussed in detail, is the lack of gauge invariance, when only contributions from one-loop box diagrams to the decay $K_L \rightarrow e\mu$ are

considered. Studies on the $K^0\bar{K}^0$ system revealed [8,18,19] that box diagrams by themselves do not form a gauge-invariant set of loop graphs in the left-right models. In addition to the box graphs, one has to take into account self-energy and vertex corrections involving very heavy Higgs bosons, which mediate flavour-changing neutral currents (FCNC). Even if the FCNC Higgs bosons were taken to have all infinite masses, their effect would not decouple from the loop. In the infinite mass limit for the heavy Higgs scalars, the residual terms are also gauge dependent and cancel against similar gauge-dependent terms coming from the box graphs, leading eventually to a gauge-invariant result. While the inclusion of the gauge-dependent Higgs self-energies to the $K_L K_S$ mass difference leads to little change in the value predicted by the box graphs, the situation for the decay $K_L \rightarrow e\mu$ is strikingly different. We find that the residual gauge-dependent terms originating from the self-energy and vertex graphs may be comparable to or even larger than the box corrections. As a consequence, the constraints on the parameter space of the left-right models will now become much more severe than those obtained in earlier articles [9,10]. Our calculation of the gauge-independent decay amplitude for $K_L \rightarrow e\mu$ at one loop and the analysis of its immediate phenomenological consequence constitute novel aspects for the left-right models, which have not been studied in detail before.

The paper is organized as follows: In Section 2, we describe the basic low-energy structure of the left-right models and review many useful relations among mixing parameters and neutrino masses, as well as relations involving gauge- and Higgs-boson masses. In Section 3, we calculate the matrix element for the decay $K_L \rightarrow e\mu$ and derive mass limits on the FCNC Higgs masses from the tree-level contribution and other theoretical considerations. All relevant Feynman rules and one-loop analytic expressions pertaining to $K_L \rightarrow e\mu$ are given in Appendices A and B, respectively. In Section 4, we show how gauge independence gets restored, when Higgs-mediated self-energy and vertex graphs are taken into account in addition to the box diagrams within the well-defined on-shell skeleton renormalization scheme. A detailed discussion on the dependence of $B(K_L \rightarrow e\mu)$ on various kinematic parameters follow in Section 5. Numerical estimates for the actual size of $B(K_L \rightarrow e\mu)$ are given within manifest as well as non-manifest left-right symmetric models. This enables one to deduce combined constraints on the parameters of these models. Our conclusions are summarized in Section 6.

2 $SU(2)_R \otimes SU(2)_L \otimes U(1)_{(B-L)}$ model

The idea of having spontaneous breakdown of both gauge and discrete symmetries can naturally be realized in left-right theories based on the gauge group $SU(2)_R \otimes SU(2)_L \otimes U(1)_{(B-L)}$

[20,21,11], where B and L denote baryon and lepton numbers, respectively. Such a realization may arise from the low-energy limit of SO(10) grand unified theories. Specifically, one of the most appealing breaking patterns of SO(10) down to the SM is the following:

$$\begin{aligned} \text{SO}(10) &\rightarrow \text{SU}(4)_{\text{PS}} \otimes \text{SU}(2)_R \otimes \text{SU}(2)_L \rightarrow \text{SU}(3)_c \otimes \text{SU}(2)_R \otimes \text{SU}(2)_L \otimes \text{U}(1)_{(B-L)} \\ &\rightarrow \text{SU}(3)_c \otimes \text{SU}(2)_L \otimes \text{U}(1)_Y. \end{aligned} \quad (2.1)$$

Among the several Higgs scalar representations which can lead to the SM, we shall adopt the field content of the left-right model introduced first in [11], which includes heavy Majorana neutrinos.

We will now describe the basic low-energy structure of the left-right models. In a three-generation left-right model, the left-handed and right-handed chiral fields are grouped in separate weak iso-doublets as follows:

$$L'_L = \begin{pmatrix} \nu'_l \\ l' \end{pmatrix}_L : (0, 1/2, -1) \quad L'_R = \begin{pmatrix} \nu'_l \\ l' \end{pmatrix}_R : (1/2, 0, -1), \quad (2.2)$$

$$Q'_L = \begin{pmatrix} u' \\ d' \end{pmatrix}_L : (0, 1/2, 1/3) \quad Q'_R = \begin{pmatrix} u' \\ d' \end{pmatrix}_R : (1/2, 0, 1/3), \quad (2.3)$$

where the weak eigenstates are denoted by a prime. In Eq. (2.2), we have also indicated the assignment of quantum numbers to fermions under the gauge group $\text{SU}(2)_R \otimes \text{SU}(2)_L \otimes \text{U}(1)_{(B-L)}$. Evidently, the above left-right symmetric extension of the SM gauge sector requires the presence of right-handed neutrinos.

The Higgs fields introduced into the model to break left-right gauge symmetry down to $\text{U}(1)_{em}$ [11] are:

$$\Phi = \begin{pmatrix} \phi_1^0 & \phi_1^+ \\ \phi_2^- & \phi_2^0 \end{pmatrix}, \quad \Delta_L = \begin{pmatrix} \delta_L^+/\sqrt{2} & \delta_L^{++} \\ \delta_L^0 & -\delta_L^+/\sqrt{2} \end{pmatrix}, \quad \Delta_R = \begin{pmatrix} \delta_R^+/\sqrt{2} & \delta_R^{++} \\ \delta_R^0 & -\delta_R^+/\sqrt{2} \end{pmatrix}, \quad (2.4)$$

where Φ is a $(1/2^*, 1/2, 0)$ Higgs bidoublet, and Δ_L and Δ_R are two complex Higgs triplets with quantum numbers $(0, 1, 2)$ and $(1, 0, 2)$, respectively. To avoid excessive complication, we will assume that only ϕ_1^0 and δ_R^0 acquire vacuum expectation values (VEV's): $\langle \phi_1^0 \rangle = \kappa_1/\sqrt{2}$ and $\langle \delta_R^0 \rangle = v_R/\sqrt{2}$. Such a scheme is also favoured for phenomenological reasons [22]. At the tree level [23,8], the vanishing of the VEV's for the neutral fields ϕ_2^0 and δ_L^0 can be achieved by imposing invariance of the left-right symmetric Higgs potential under the discrete symmetry $D: \Phi \rightarrow i\Phi, \Delta_L \rightarrow \Delta_L$ and $\Delta_R \rightarrow -\Delta_R$. As has been observed in [24], however, the D symmetry may suppress unnaturally large FCNC's but leads to zero masses for the down quarks and the charged leptons. Even though the latter may be

viewed as a viable approximation for $K_L \rightarrow e\mu$, the presence of non-zero m_{d_i} and m_{l_i} would require infinite renormalization of the VEV of δ_L^0 . To overcome this problem, the authors in [24] suggested that stability of such a model under high order quantum corrections can naturally be achieved within a D-parity breaking scenario. Since we shall treat charged leptons and down-type quarks as being strictly massless at the quantum level, the above problem does not occur in our calculations.

The left-right scenario of our interest is further described in Ref. [22], under case (d). The fact that $\langle \delta_L^0 \rangle = \langle \phi_2^0 \rangle = 0$ in this case implies the absence of mixing between the charged gauge bosons W_L^+ and W_R^+ . Thus, W_L^+ may be identified as the known W^+ boson with mass M_W observed experimentally, whereas W_R^+ is an extra gauge boson having a mass M_R larger than at least 0.5 TeV [1]. In addition, the minimal left-right model predicts two massive neutral gauge bosons, Z_L and Z_R , which have a non-vanishing tree-level mixing of order $\kappa_1^2/v_R^2 \sim 10^{-2}$. Nevertheless, $Z_{L,R}$ -mediated interactions are not of much relevance here, since they do not directly enter our discussion of $K_L \rightarrow e\mu$.

The scalar spectrum of the left-right model consists of 20 degrees of freedom, of which six degrees become the longitudinal components of the gauge bosons: W_L^\pm , W_R^\pm , Z_L and Z_R . From the remaining 14 physical states, only the charged scalars h^\pm , the CP-even Higgs boson $\phi_2^r = \Re e\phi_2^0/\sqrt{2}$ and the CP-odd Higgs scalar $\phi_2^i = \Im m\phi_2^0/\sqrt{2}$ are of direct relevance to the decay $K_L \rightarrow e\mu$. The field h^+ is the orthogonal component of the right-handed would-be Goldstone boson G_R^+ . The fields h^+ and G_R^+ are not pure mass-eigenstates but admixtures of ϕ_1^+ and δ_R^+ , *viz.*

$$\begin{pmatrix} h^+ \\ G_R^+ \end{pmatrix} = \begin{pmatrix} c_\beta & s_\beta \\ -s_\beta & c_\beta \end{pmatrix} \begin{pmatrix} \phi_1^+ \\ \delta_R^+ \end{pmatrix}, \quad s_\beta = \sqrt{1 - c_\beta^2} = \frac{M_W}{M_R}. \quad (2.5)$$

As we will see in Section 3, the scalars $\phi_2^{r,i}$ must be very heavy, *i.e.*, heavier than 10 TeV, in order to avoid large FCNC contributions to the $K_L K_S$ mass difference. Furthermore, after diagonalization of the relevant mass matrices, h^\pm and $\phi_2^{r,i}$ are found to be nearly degenerate [22]. In fact, one obtains

$$M_{\phi_2^r}^2 = M_{\phi_2^i}^2 + \mathcal{O}(M_W^2) = M_h^2 + \mathcal{O}(M_W^2) \quad (2.6)$$

Therefore, it is reasonable to assume that the Higgs scalars h^\pm , ϕ_2^r and ϕ_2^i are *exactly* degenerate.

The left-right model admits the presence of $B - L$ -violating operators in the Yukawa sector, which are introduced by the triplet fields $\Delta_{L,R}$ in the following way:

$$\mathcal{L}_{\text{int}}^{B-L} = -\frac{\sqrt{2}m_{M_{ij}}}{2v_R} \left(h_{ij} \bar{L}_{L_i}^{\prime C} \varepsilon_{ij} \Delta_L L'_{L_j} + \bar{L}_{R_i}^{\prime C} \varepsilon_{ij} \Delta_R L'_{R_j} \right) + \text{H.c.}, \quad (2.7)$$

where ε_{ij} is the usual Levi-Civita tensor, m_{Mij} are Majorana mass terms and h_{ij} are Yukawa couplings, which are much smaller than unity owing to phenomenological constraints from muon and τ decays [22]. After spontaneous symmetry breaking, the Lagrangian describing the neutrino mass matrix is given by

$$\begin{aligned}\mathcal{L}_{\text{mass}}^\nu &= -\frac{1}{2} (\bar{\nu}'_L, \bar{\nu}'_R{}^C) M^\nu \begin{pmatrix} \nu'_L{}^C \\ \nu'_R \end{pmatrix} + \text{H.c.} \\ &= -\frac{1}{2} \bar{n}_L \widehat{M}^\nu n_R + \text{H.c.},\end{aligned}\tag{2.8}$$

where the 6×6 -dimensional matrix M^ν takes on the known see-saw-type form, *i.e.*,

$$M^\nu = \begin{pmatrix} 0 & m_D \\ m_D^T & m_M \end{pmatrix}.\tag{2.9}$$

The Dirac mass matrix m_D is a 3×3 -dimensional matrix originating from the breaking of the $SU(2)_L$ sector. In general, the matrix M^ν is always diagonalizable by a 6×6 unitary matrix U^ν through

$$U^{\nu T} M^\nu U^\nu = \widehat{M}^\nu.\tag{2.10}$$

After diagonalization, one gets six physical Majorana neutrinos n_i . Three of the six mass-eigenstates are assigned to the ordinary light neutrinos, ν_e , ν_μ and ν_τ , while the remaining three states, N_1 , N_2 and N_3 , describe new Majorana neutrinos, which must be heavier than about 100 GeV for phenomenological reasons [26].

By analogy, the 3×3 charged-lepton mass matrix M^l can always be diagonalized through the bi-unitary transformation

$$V_L M^l V_R^\dagger = \widehat{M}^l,\tag{2.11}$$

where V_L and V_R are unitary matrices that relate the weak fields l'_L and l'_R to the mass eigenstates l_L and l_R , respectively. Adopting the conventions of Ref. [26], we can now write the charged-current interaction of the Majorana neutrinos n_i and charged leptons l_i with the left-handed gauge boson W_L^\pm ($\equiv W^\pm$). The charged-current Lagrangian is given by

$$\mathcal{L}_{\text{int}}^{W_L} = -\frac{g_w}{\sqrt{2}} W_L^{-\mu} B_{li}^L \bar{l} \gamma_\mu P_L n_i + \text{H.c.},\tag{2.12}$$

where g_w is the weak coupling constant, $c_w^2 = 1 - s_w^2 = M_W^2/M_Z^2$, $P_{L(R)} = [1 - (+)\gamma_5]/2$ and B^L is the 3×6 matrix

$$B_{ij}^L = \sum_{k=1}^3 V_{L_{ik}} U_{kj}^{\nu*},\tag{2.13}$$

which describes the mixing of the left-handed charged leptons with the neutrinos. Furthermore, the Z_L boson couples to the Majorana neutrinos through the 6×6 mixing matrix

$$C_{ij}^L = \sum_{k=1}^3 U_{ki}^\nu U_{kj}^{\nu*}. \quad (2.14)$$

In an analogous way, the mixing matrices B_{li}^R and C_{ij}^R ,

$$B_{lj}^R = \sum_{k=4}^6 V_{Rlk} U_{kj}^\nu \quad \text{and} \quad C_{ij}^R = \sum_{k=4}^6 U_{ki}^{\nu*} U_{kj}^\nu, \quad (2.15)$$

mediate the interactions of the W_R^\pm and Z_R bosons to the charged leptons and Majorana neutrinos. In the left-right models, the quark sector is modified as well, namely, there are additional couplings of the fermionic fields to the gauge and extra Higgs bosons. All Feynman rules that are necessary for the calculation of $K_L \rightarrow e\mu$ are relegated to Appendix A.

The left-handed flavour-mixing matrices B^L and C^L , which are identical to the respective mixing matrices B and C of the SM with right-handed neutrinos, satisfy a number of identities that may be found in [26,14]. In addition, the right-handed mixing matrices B^R and C^R obey the relations [17]:

$$\sum_{i=1}^6 B_{l_1 i}^L B_{l_2 i}^R = 0, \quad \sum_{l=1}^3 B_{li}^{R*} B_{lj}^R = C_{ij}^R, \quad C_{ij}^{L*} + C_{ij}^R = \delta_{ij}. \quad (2.16)$$

These identities is a direct consequence of the unitarity of the theory, assuring its renormalizability. To simplify further the analysis of $K_L \rightarrow e\mu$, we shall assume that only the electron and muon families mix effectively, whereas the τ family stays unmixed. In such an effective two-generation-mixing model, one obtains [13,14]

$$B_{lN_1}^L = \frac{\rho^{1/4} s_L^{\nu_l}}{\sqrt{1 + \rho^{1/2}}}, \quad B_{lN_2}^L = \frac{i s_L^{\nu_l}}{\sqrt{1 + \rho^{1/2}}}, \quad (2.17)$$

where the ratio $\rho = m_{N_2}^2/m_{N_1}^2$ is always understood to be greater or equal than unity and $s_L^{\nu_l}$ (with $l = e, \mu$) are the light-heavy neutrino mixings introduced in [27], *i.e.*,

$$(s_L^{\nu_l})^2 \equiv \sum_{i=1}^2 |B_{lN_i}^L|^2 \simeq \left(m_D^\dagger \frac{1}{m_M^2} m_D \right)_{ll}. \quad (2.18)$$

In addition, for the mixings $C_{N_i N_j}^L$, one finds

$$\begin{aligned} C_{N_1 N_1}^L &= \rho^{1/2} C_{N_2 N_2}^L = \frac{\rho^{1/2}}{1 + \rho^{1/2}} [(s_L^{\nu_e})^2 + (s_L^{\nu_\mu})^2], \\ C_{N_1 N_2}^L &= -C_{N_2 N_1}^L = i \rho^{1/4} C_{N_2 N_2}^L. \end{aligned} \quad (2.19)$$

Finally, with the help of Eq. (2.16) together with Eq. (2.15), we can find the mixings $B_{lN_i}^R$ up to an arbitrary Cabbibo-type angle θ_R [17]. The mixings $B_{lN_i}^R$ are given by

$$\begin{aligned}
B_{l_1 N_1}^R &= \cos \theta_R \sqrt{1 - C_{N_1 N_1}^L}, & B_{l_2 N_1}^R &= -\sin \theta_R \sqrt{1 - C_{N_1 N_1}^L}, \\
B_{l_1 N_2}^R &= -\cos \theta_R \frac{C_{N_2 N_1}^L}{\sqrt{1 - C_{N_1 N_1}^L}} - i \sin \theta_R \left[\frac{(1 - C_{N_1 N_1}^L)(1 - C_{N_2 N_2}^L) - |C_{N_1 N_2}^L|^2}{1 - C_{N_1 N_1}^L} \right]^{1/2}, \\
B_{l_2 N_2}^R &= \sin \theta_R \frac{C_{N_2 N_1}^L}{\sqrt{1 - C_{N_1 N_1}^L}} - i \cos \theta_R \left[\frac{(1 - C_{N_1 N_1}^L)(1 - C_{N_2 N_2}^L) - |C_{N_1 N_2}^L|^2}{1 - C_{N_1 N_1}^L} \right]^{1/2}. \quad (2.20)
\end{aligned}$$

Counting now the number of independent kinematic parameters present in the leptonic sector of our two-generation left-right model, we find five free quantities: the masses of the two heavy Majorana neutrinos, m_{N_1} and m_{N_2} [or equivalently m_{N_1} and ρ], the two light-heavy neutrino mixings, $(s_L^{\nu_e})^2$ and $(s_L^{\nu_\mu})^2$, which are severely constrained by low-energy data as we will see later on in this section, and the angle θ_R .

It is now interesting to remark that M^ν in Eq. (2.9) reduces to the traditional seesaw scheme [12] in the limit $m_M \gg m_D$. In the see-saw mass pattern, the light-heavy neutrino mixings $s_L^{\nu_i}$ are very suppressed, since they are governed from the relation $s_L^{\nu_i} \sim \sqrt{m_{\nu_i}/m_N}$. The usual seesaw models predict very small rates for lepton-flavour-violating decays, such as $K_L \rightarrow e\mu$, $\mu \rightarrow eee$, *etc.*, which are beyond the realm of detection in any foreseeable experiment. The situation may change drastically if a non-trivial mixing between two families [28] is introduced. To give an example, consider the following Dirac and Majorana sub-matrices in Eq. (2.9):

$$m_D = \begin{pmatrix} 0 & a \\ 0 & b \end{pmatrix}, \quad m_M = \begin{pmatrix} 0 & A \\ A & \mu \end{pmatrix}, \quad (2.21)$$

where a , b , A and μ are arbitrary complex numbers. It is then easy to verify that the rank of the 4×4 matrix M^ν is two. This implies that two eigenstates are exactly massless at the tree level, whereas the other two are massive. The scheme in Eq. (2.21) may also be derived from an horizontal symmetry, which is broken softly by a lepton-number-violating operator proportional to μ . In fact, if μ arises from the spontaneous breakdown of a global symmetry, then it should be $\mu \ll A$ in order to avoid large Majoron couplings to electron and u , d quarks, as is required from astrophysical considerations [25]. In this scenario, the light neutrinos acquire masses radiatively in agreement with experimental upper bounds [26]. Most importantly, the mixings $s_L^{\nu_i}$ now scale as $s_L^{\nu_i} \sim a/A$, b/A and therefore are large. In particular, we should note that the derivation of the mixings B^L and B^R in Eqs. (2.17) and (2.20) are based on non-seesaw scenarios of the generic form (2.21). These mixings can only be constrained from a global analysis of low-energy data.

There are many experimental data that can be used to constrain the light-heavy neutrino mixings [27]. Here, we shall however focus only on those limits that involve the e and μ families and are relevant for the decay $K_L \rightarrow e\mu$. We shall also assume that the two heavy Majorana neutrinos N_1 and N_2 are almost degenerate in mass, namely, $m_{N_1} = m_{N_2} = m_N$. Thus, charged current universality in π decays [29] and in the decay $\mu \rightarrow e\nu\nu$ [1] lead to the limits:

$$(s_L^{\nu_e})^2, (s_L^{\nu_\mu})^2 < 0.010. \quad (2.22)$$

Furthermore, in the large m_N limit, heavy Majorana neutrinos give rise to $\mu \rightarrow e\gamma$ decays with branching ratio

$$B(\mu \rightarrow e\gamma) = \frac{3\alpha_{em}}{8\pi} (s_L^{\nu_e})^2 (s_L^{\nu_\mu})^2. \quad (2.23)$$

On the experimental side, $B_{\text{exp}}(\mu \rightarrow e\gamma) \leq 4.9 \times 10^{-11}$, which yields the tight constraint:

$$(s_L^{\nu_e})^2 (s_L^{\nu_\mu})^2 < 5.6 \times 10^{-8}. \quad (2.24)$$

For the model at hand, the absence of $\mu - e$ conversion events in nuclei [30] may lead to more stringent bounds due to the non-decoupling behaviour of the heavy neutrinos in the $Ze\mu$ coupling [15]. A first estimate gives

$$\frac{1}{2} s_L^{\nu_e} s_L^{\nu_\mu} [(s_L^{\nu_e})^2 + (s_L^{\nu_\mu})^2] \lesssim 10^{-6} \times \frac{M_W^2}{m_N^2}. \quad (2.25)$$

If the heavy neutrinos have TeV mass, both constraints (2.24) and (2.25) are then comparable. For very heavy neutrinos of order 10 TeV, the bound due to $\mu - e$ conversion is more restrictive. Of course, one can completely avoid the latter constraint by assuming, for example, that the muon number is practically conserved by the left-handed interactions, which merely means that $b \ll a$ in Eq. (2.21). Even if one takes $s_L^{\nu_\mu} = 0$, $K_L \rightarrow e\mu$ can still proceed via the exchange of W_L^+ and W_R^+ bosons in the loop. Finally, we find that the decay $\mu \rightarrow eee$ provides in general a weaker constraint than that given in Eq. (2.25).

In the see-saw type matrix (2.9), the Dirac and Majorana mass terms, m_D and m_M , cannot be arbitrarily large but are constrained from above by triviality and perturbative unitarity bounds. Renormalization-group-triviality bounds, which are mainly controlled by large contributions to the quartic scalar couplings in the Higgs potential, usually lead to the limit: $m_D < 2M_W/g_w \approx 300$ GeV. However, the coexistence of large Majorana masses $m_M \gg m_D$ in the loop of the Higgs potential will screen the one-loop contributions of the heavy neutrinos to the Higgs potential considerably. In fact, the low-energy data mentioned above require $m_D/m_M < 10^{-1}$. Therefore, a more reliable constraint arises due

to perturbative unitarity, where the inequality $\Gamma(N \rightarrow lW_L^+, \nu Z_L) < m_N/2$ is imposed. This inequality amounts to the bound

$$m_D \lesssim 10 M_W. \quad (2.26)$$

Similarly, the Majorana mass m_M may be constrained from an analogous inequality $\Gamma(N \rightarrow lW_R^+, \nu Z_R) < m_N/2$, which gives the bound

$$m_M \lesssim 10 M_R. \quad (2.27)$$

The limits derived in Eqs. (2.26) and (2.27) are used throughout our analysis.

3 Matrix element of $K_L \rightarrow e\mu$

In the left-right models, the lepton-flavour violating decay $K_L \rightarrow e\mu$ can occur at the tree level via the exchange of FCNC Higgs scalars, as shown in Fig. 1. However, for very heavy FCNC Higgs masses, the tree-level contribution gets rather suppressed due to the intermediate Higgs-boson propagator, while one-loop graphs shown in Figs. 2–4 can, in principle, become very significant, since they do not depend explicitly on the FCNC Higgs masses. Therefore, we shall include in our study all the relevant one-loop diagrams contributing to $K_L \rightarrow e\mu$.

The one-loop matrix element of the decay $K_L \rightarrow e\mu$ has the general form

$$\mathcal{T}(\bar{K}^0 \rightarrow e^+\mu^-) = \frac{1}{(4\pi)^2} \left(\frac{g_w}{\sqrt{2}} \right)^4 \frac{1}{M_W^2} \langle 0 | \bar{d}\gamma_\kappa P_L s | \bar{K}^0 \rangle \bar{u}_\mu \gamma^\kappa P_L v_e (\mathcal{A} + \eta \mathcal{B}), \quad (3.1)$$

where the reduced amplitudes \mathcal{A} and \mathcal{B} are given in Appendix B. The parameter η in Eq. (3.1) is an enhancement factor originating from chirality-flipping operators which enter in the kaon-to-vacuum matrix element. The factor η is given by

$$\begin{aligned} \eta &= \frac{\langle 0 | \bar{d}\gamma^\sigma \gamma^\kappa P_R s | \bar{K}^0 \rangle \bar{u}_\mu \gamma_\sigma \gamma_\kappa P_L v_e}{\langle 0 | \bar{d}\gamma^\alpha P_L s | \bar{K}^0 \rangle \bar{u}_\mu \gamma_\alpha P_L v_e} \\ &\simeq \frac{4M_K^2}{(m_s + m_d)m_\mu} \simeq 50, \end{aligned} \quad (3.2)$$

where M_K is the mass of K^0 , and m_d and m_s denote the current d - and s -quark masses, respectively [31]. In the derivation of the parameter η in Eq. (3.2), we have taken into account the PCAC hypothesis and the fact that

$$\langle 0 | \bar{d}\gamma_\mu \gamma_\nu P_R s | \bar{K}^0(p) \rangle = g_{\mu\nu} \langle 0 | \bar{d}\gamma_5 s | \bar{K}^0(p) \rangle + \frac{1}{2} \langle 0 | \bar{d}[\gamma_\mu, \gamma_\nu] \gamma_5 s | \bar{K}^0(p) \rangle. \quad (3.3)$$

The second term on the RHS of Eq. (3.3) must be a Lorentz tensor antisymmetric in $p^\mu p^\nu$ and hence vanishes identically. Applying the PCAC hypothesis to the hadronic matrix element

$$\langle 0 | \bar{d}(x) \gamma_\mu \gamma_5 s(x) | \bar{K}^0(p) \rangle = i p_\mu f_K e^{-ipx}, \quad (3.4)$$

where f_K is the kaon decay constant, we can calculate the matrix element

$$\langle 0 | \bar{d}(x) \gamma_5 s(x) | \bar{K}^0(p) \rangle = -i \frac{M_K^2 f_K}{m_d + m_s} e^{-ipx}. \quad (3.5)$$

Using the relations (3.3), (3.4), (3.5) and little algebra, the second equality in Eq. (3.2) follows easily.

Substituting Eq. (3.4) into Eq. (3.1), we find the branching ratio

$$B(K_L \rightarrow e\mu) = 4.1 \times 10^{-4} |\mathcal{A} + \eta \mathcal{B}|^2, \quad (3.6)$$

where the charge of the leptons in the final state is not tagged. One arrives at the same result for $B(K_L \rightarrow e\mu)$ in Eq. (3.6), by using relations based on isospin invariance between the decay amplitudes of $\bar{K}^0 \rightarrow \mu^- e^+$ and $K^- \rightarrow \mu^- \nu_\alpha$.

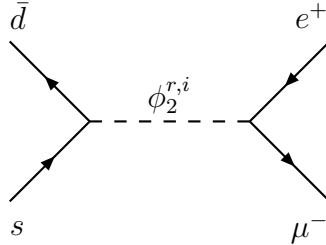


Fig. 1: Tree-level graph contributing to $K_L \rightarrow e\mu$

The tree-level $\phi_2^{r,i}$ -exchange shown in Fig. 1 gives rise to a contribution to $\mathcal{T}(\bar{K}^0 \rightarrow e\mu)$, which is proportional to the reduced amplitude

$$\begin{aligned} \mathcal{B}_{\text{tree}} &= \frac{\pi}{\alpha_w} \sum_{i=c,t} \sum_{\alpha=1}^6 (\lambda_i \lambda_\alpha)^{1/2} \left[\frac{1}{\lambda_R} \left(V_{id}^{L*} V_{is}^R B_{\mu\alpha}^L B_{e\alpha}^{R*} + V_{id}^{L*} V_{is}^R B_{\mu\alpha}^R B_{e\alpha}^{L*} + (L \leftrightarrow R) \right) \right. \\ &\quad \left. + \frac{1}{\lambda_I} \left(V_{id}^{L*} V_{is}^R B_{\mu\alpha}^L B_{e\alpha}^{R*} - V_{id}^{L*} V_{is}^R B_{\mu\alpha}^R B_{e\alpha}^{L*} + (L \leftrightarrow R) \right) \right], \end{aligned} \quad (3.7)$$

whereas $\mathcal{A}_{\text{tree}} = 0$. In Eq. (3.7), we have defined $\lambda_{c,t} = m_{c,t}^2/M_W^2$, $\lambda_\alpha = m_{n_\alpha}^2/M_W^2$, $\lambda_R = M_{\phi_2^r}^2/M_W^2$ and $\lambda_I = M_{\phi_2^i}^2/M_W^2$.

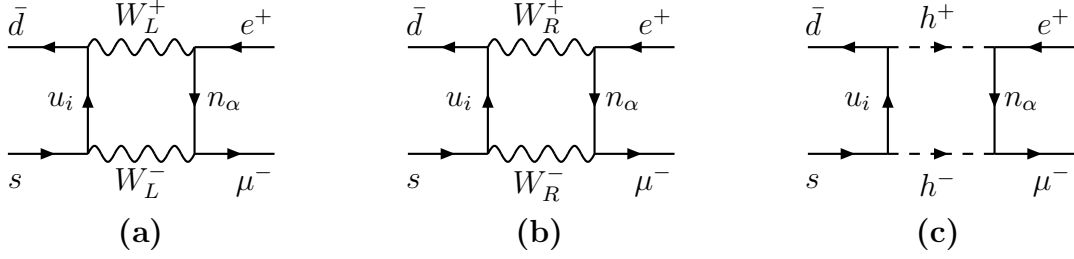


Fig. 2: Gauge-independent sub-set of Feynman graphs (group A) contributing to $K_L \rightarrow e\mu$

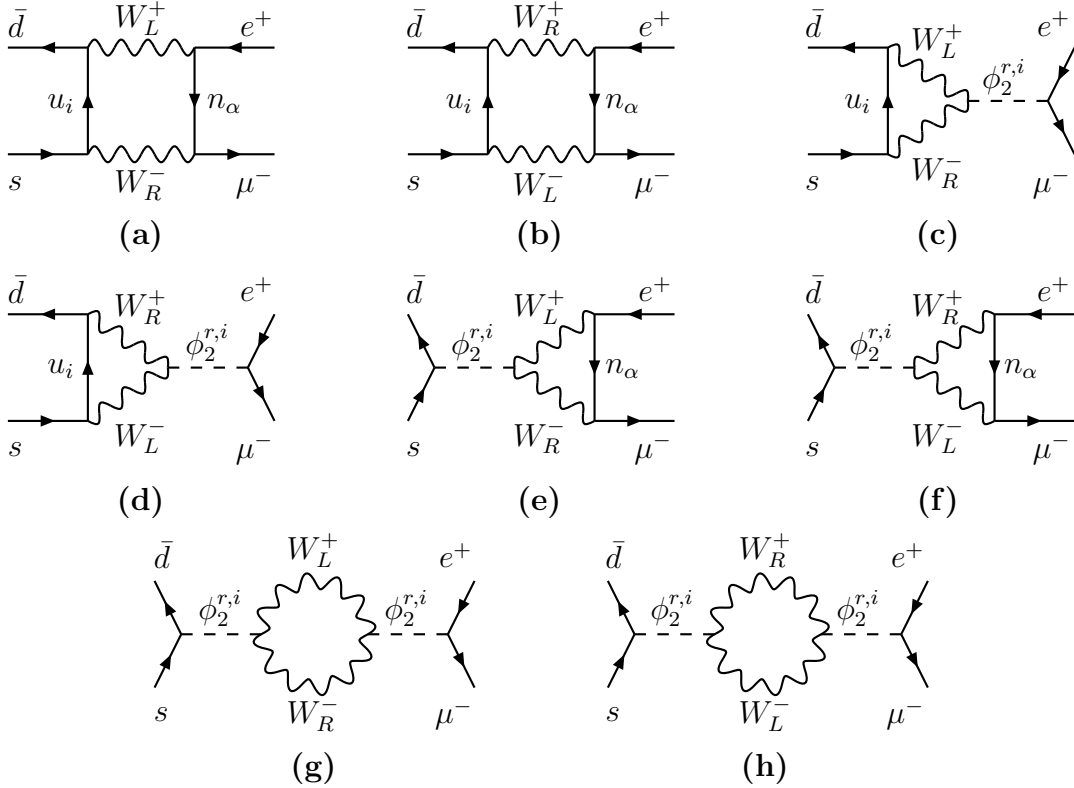


Fig. 3: Gauge-independent sub-set of Feynman graphs (group B) contributing to $K_L \rightarrow e\mu$

There are tight experimental constraints on the masses of the FCNC scalars and the mixing angles, which depend on the flavour structure of the left-right model. For example, in non-manifest left-right models [9], the experimental limit coming from the mass difference between K_L and K_S leads to the lower mass bound

$$M_{\phi_2^r} \sim M_{\phi_2^i} \gtrsim 9 \text{ TeV}. \quad (3.8)$$

If we impose a manifest left right-symmetry on the model, *i.e.*, $V^L = V^R = V$, the mass bound (3.8) is even more severe, and the FCNC scalars must be heavier than 30 TeV [32].

On the other hand, in the manifest left-right symmetric model, the tree-level contribution to $K_L \rightarrow e\mu$ yields the following constraint:

$$M_{\phi_2^{r,i}} \gtrsim 35 \left(\frac{V_{td}}{0.015} \right)^{1/2} \left(\frac{V_{ts}}{0.048} \right)^{1/2} \left(\frac{s_L^{\nu_i}}{0.01} \right)^{1/2} \left(\frac{m_t}{180 \text{ GeV}} \right)^{1/2} \left(\frac{m_N}{10 \text{ TeV}} \right)^{1/2} \text{ TeV}, \quad (3.9)$$

which is comparable to the one obtained from the $K_L K_S$ mass difference.

Another important bound comes from the requirement that the validity of perturbative expansion be preserved. The unitarity bound derived in this way is translated into the approximate inequality [33]

$$M_{\phi_2^{r,i}} \lesssim 15 M_R. \quad (3.10)$$

The above bound will be considered throughout our phenomenological analysis in Section 5.

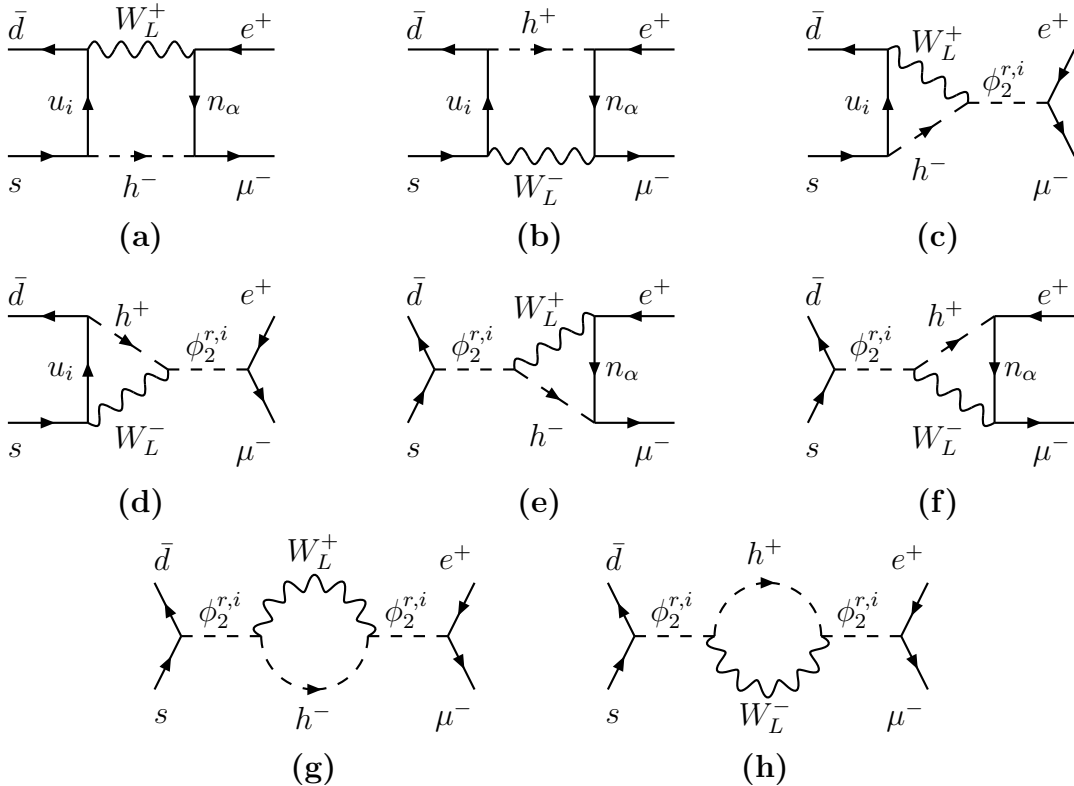


Fig. 4: Gauge-independent sub-set of Feynman graphs (group C) contributing to $K_L \rightarrow e\mu$

If the FCNC Higgs scalars are sufficiently heavy, *e.g.* much heavier than 10 TeV according to Eqs. (3.8) and (3.9), the tree-level contribution to $\mathcal{T}(\bar{K}^0 \rightarrow e\mu)$ may become smaller than the present experimental limits. However, the one-loop box diagrams shown

in Figs. 2–5, being independent of the heavy neutral Higgs masses, can still give significant contributions to the decay $K_L \rightarrow e\mu$. Therefore, the impact of the loop corrections on the phenomenological predictions should be studied very carefully. Thereby it should be kept in mind that the box diagrams alone do not form a gauge-invariant set, but vertex and Higgs vacuum polarization graphs must be included. This issue together with that of renormalization will be discussed in detail in the next section.

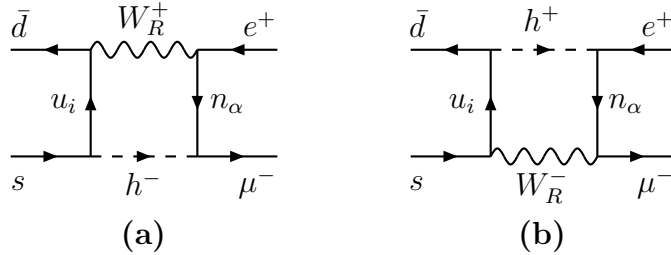


Fig. 5: Gauge-independent sub-set of Feynman graphs (group D) contributing to $K_L \rightarrow e\mu$

4 Gauge independence and renormalization

In general, the W_R^\pm and W_L^\pm propagators depend on the gauge used to remove the unphysical degrees of freedom and on the parameter chosen for fixing such a gauge. There are many gauges to carry out this procedure, such as covariant R_ξ gauges, non-covariant axial gauges, *etc.* Hence, the W_R^\pm and W_L^\pm propagators may introduce gauge-fixing-parameter dependence if only an arbitrary sub-set of loop graphs is considered. For example, considering box graphs only to describe the $K^0\bar{K}^0$ mixing in left-right models is found to be insufficient to cancel such a dependence on the gauge-fixing parameter ξ [8,18,19,9].

In the following, we shall closer examine the gauge dependence of $\mathcal{T}(\bar{K}^0 \rightarrow e^+\mu^-)$ on the W_L and W_R propagators in the covariant R_ξ gauge. The R_ξ gauge may be viewed as the most practicable class of gauges endowed with the manifest properties of Lorentz invariance and renormalizability. In particular, we wish to identify all those diagrams, which, together with the box graphs, form a minimal gauge-independent set. To this end, we have divided all the radiative corrections into four groups A–D, depending on the way that the W_R and W_L propagators enter in the loop. These assignments are represented in Figs. 2–5. It is then not difficult to verify that the groups of box graphs A and D are separately independent of the gauge-fixing parameter ξ . In the other classes of graphs, *i.e.*, B and C, however, one must consider additional diagrams containing FCNC Higgs scalars and all relevant tadpoles, which are not shown in Figs. 3 and 4. Since the self-energy

diagrams in groups B and C are UV infinite, we will simplify our task by proving gauge independence after renormalization. This is indeed a rather economical way to check ξ independence, since a vast number of tadpoles, being momentum independent, will drop out, when all relevant renormalization subtractions are performed. For that purpose, we shall adopt the on-shell skeleton (OSS) renormalization scheme, which is also discussed in Ref. [19].

The main virtue of the OSS scheme is its explicit maintenance of gauge independence during the process of renormalization. The OSS renormalization is based on subtracting lower n -point correlation functions from the transition amplitude under consideration. The lower n -point correlation functions, which normally represent self-energy and vertex graphs, are formally gauge independent, since they are evaluated at on-shell external momenta. More explicitly, the OSS scheme may be described as follows. Whenever we have to renormalize a vertex sub-graph, *e.g.*, the one-loop $\phi_2^r \mu^- e^+$ coupling $\Gamma_{\phi_2^r}(p^2)$ shown in Figs. 4(c) and 4(d), we have just to make the subtraction

$$\Gamma_{\phi_2^r}^{R1}(p^2) = \Gamma_{\phi_2^r}(p^2) - \Gamma_{\phi_2^r}(M_{\phi_2^r}^2). \quad (4.1)$$

The above operation is called *R1* subtraction. By analogy, we renormalize all the self-energy graphs involving the FCNC Higgs bosons, *e.g.*, $\Pi_{\phi_2^r}(p^2)$ in Figs. 4(g) and 4(h), by making two subtractions defined as

$$\Pi_{\phi_2^r}^{R2}(p^2) = \Pi_{\phi_2^r}(p^2) - \Pi_{\phi_2^r}(M_{\phi_2^r}^2) - (p^2 - M_{\phi_2^r}^2) \frac{d}{dp^2} \Pi_{\phi_2^r}(p^2) \Big|_{p^2=M_{\phi_2^r}^2}, \quad (4.2)$$

which is characterized as *R2* operation. In our analysis, we shall not study possible effects due to renormalization scheme dependence [34], which are of high order. In any case, the lepton-flavour-violating decay $K_L \rightarrow e\mu$ would not constitute the best place to look for such effects.

In the following, we shall see how the box graphs in class C (Fig. 4) are ξ dependent and how gauge independence gets restored if the relevant Higgs self-energies and vertex graphs are taken into account in the OSS renormalization scheme. The same procedure may be applied to the class B. The class A and D are separately gauge independent and UV finite. Obviously, OSS renormalization cannot apply to the groups A and D, since they only consist of box diagrams.

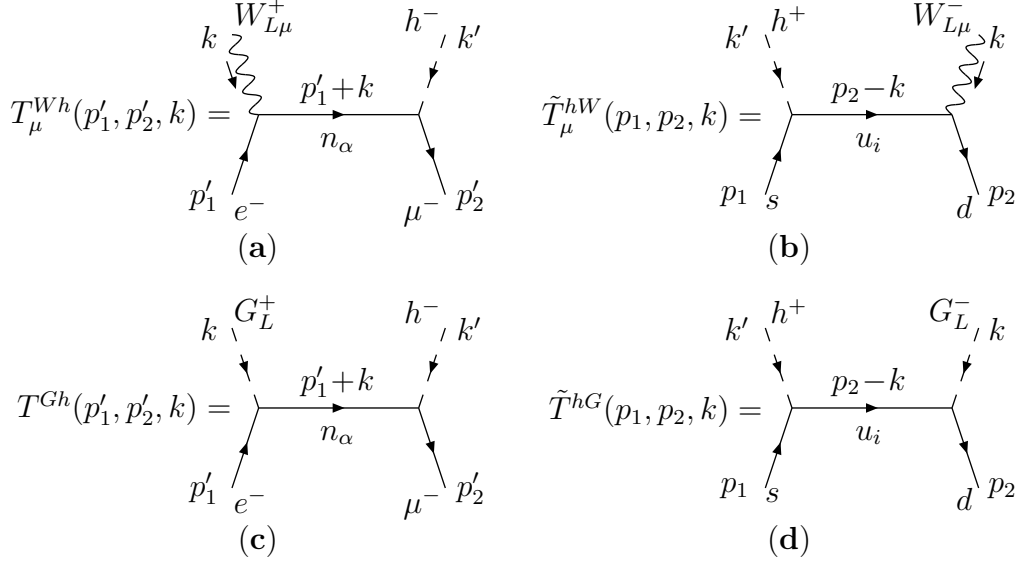


Fig. 6: Diagrammatic definitions of tree-level amplitudes pertinent to class C.

4.1 Gauge dependence of box diagrams

We start examining the gauge dependence of the box diagrams in class C shown in Fig. 4 in the R_ξ gauges. In this class of gauges, the gauge-boson propagator, *e.g.*, of the W_L boson may conveniently be decomposed as follows:

$$\Delta_{\mu\nu}(k) = U_{\mu\nu}(k) - \frac{k_\mu k_\nu}{M_W^2} \Delta_\xi(k), \quad (4.3)$$

where

$$U_{\mu\nu}(k) = \frac{1}{k^2 - M_W^2} \left(-g_{\mu\nu} + \frac{k_\mu k_\nu}{M_W^2} \right) \quad (4.4)$$

is the respective W_L -boson propagator in the unitary gauge and

$$\Delta_\xi(k) = \frac{1}{k^2 - \xi M_W^2} \quad (4.5)$$

is the ξ -dependent part of the W_L -boson propagator. Note that $\Delta_\xi(k)$ coincides with the propagators of the would-be Goldstone boson G_L and the ghost fields c_L , \bar{c}_L , which correspond to W_L . Similarly, one can perform an analogous decomposition for W_R -boson propagator, which will depend on another gauge-fixing parameter, *e.g.*, ξ' . Such a decomposition is very useful to study the gauge independence of the class B, which is, however, conceptually very similar to that of the class C considered here. Finally, the propagator for the free charged Higgs bosons h^\pm is given by

$$D_h(k) = \frac{1}{k^2 - M_h^2}, \quad (4.6)$$

which is independent of ξ .

To make use of the propagator decomposition mentioned above, we write the amplitude for the diagram (a) in Fig. 4 as a sum of two sub-amplitudes: $\mathcal{M}_a = \mathcal{M}_a^W + \mathcal{M}_a^G$. Omitting integration over the loop momentum, the sub-amplitudes are given by

$$\mathcal{M}_a^W = -T_\mu^{Wh}(k)\tilde{T}_\nu^{hW}(-k)\Delta^{\mu\nu}(k)D_h(k'), \quad (4.7)$$

$$\mathcal{M}_a^G = -T^{Gh}(k)\tilde{T}^{hG}(-k)\Delta_\xi(k)D_h(k'). \quad (4.8)$$

where k and k' are the loop momenta carried by the W_L^+ and charged Higgs bosons h^- , respectively. In Eqs. (4.7) and (4.8), T_μ^{Wh} , T_μ^{Gh} , \tilde{T}_ν^{hW} and \tilde{T}^{hG} are the tree-level amplitudes depicted in Fig. 6. These tree-level amplitudes read:

$$\begin{aligned} T_\mu^{Wh}(p'_1, p'_2, k) &= -\frac{i}{c_\beta M_W} \left(\frac{ig_w}{\sqrt{2}}\right)^2 \bar{u}_\mu(p'_2) \left[c_\beta m_\mu B_{\mu\alpha}^R P_R + (s_\beta^2 \delta_{\gamma\alpha} - C_{\gamma\alpha}^L) m_\gamma B_{\mu\gamma}^R P_L \right] \\ &\quad \times \frac{1}{\not{p}'_1 + \not{k} - m_\alpha} \gamma_\mu B_{e\alpha}^{L*} P_L v_e(p'_1), \end{aligned} \quad (4.9)$$

$$\tilde{T}_\mu^{hW}(p_1, p_2, k) = \frac{ic_\beta}{M_W} \left(\frac{ig_w}{\sqrt{2}}\right)^2 \bar{v}_d(p_2) \gamma_\mu V_{id}^{L*} \frac{1}{\not{p}'_2 - \not{k} - m_i} (m_i P_R - m_s P_L) V_{is}^R u_s(p_1), \quad (4.10)$$

$$\begin{aligned} T^{Gh}(p'_1, p'_2, k) &= -\frac{i}{c_\beta M_W^2} \left(\frac{ig_w}{\sqrt{2}}\right)^2 \bar{u}_\mu(p'_2) \left[c_\beta m_\mu B_{\mu\alpha}^R P_R + (s_\beta^2 \delta_{\gamma\alpha} - C_{\gamma\alpha}^L) m_\gamma B_{\mu\gamma}^R P_L \right] \\ &\quad \times \frac{1}{\not{p}'_1 + \not{k} - m_\alpha} B_{e\alpha}^{L*} (m_e P_R - m_\alpha P_L) v_e(p'_1), \end{aligned} \quad (4.11)$$

$$\begin{aligned} \tilde{T}^{hG}(p_1, p_2, k) &= \frac{ic_\beta}{M_W^2} \left(\frac{ig_w}{\sqrt{2}}\right)^2 \bar{v}_d(p_2) (m_d P_R - m_i P_L) V_{id}^{L*} \frac{1}{\not{p}'_2 - \not{k} - m_i} \\ &\quad \times (m_i P_R - m_s P_L) V_{is}^R u_s(p_1). \end{aligned} \quad (4.12)$$

Using the propagator decomposition of Eq. (4.3), one can now write

$$\mathcal{M}_a^W = \mathcal{M}_a^U + \mathcal{M}_a^\xi, \quad (4.13)$$

with

$$\mathcal{M}_a^U = -T_\mu^{Wh}(k)\tilde{T}_\nu^{hW}(-k)U^{\mu\nu}(k)D_h(k'), \quad (4.14)$$

$$\mathcal{M}_a^\xi = \frac{k^\mu k^\nu}{M_W^2} T_\mu^{Wh}(k)\tilde{T}_\nu^{hW}(-k)\Delta_\xi(k)D_h(k'). \quad (4.15)$$

Here, \mathcal{M}_a^U denotes the amplitude of box diagram 4(a) in the unitary gauge, which does not explicitly depend on the gauge parameter ξ . In the unitary gauge, the unphysical Goldstone bosons (and ghosts) are absent.

The tree-level amplitudes given in Fig. 6 satisfy the following Ward identities:

$$\frac{k^\mu}{M_W} T_\mu^{Wh}(k) = -T^{Gh} - E_L, \quad (4.16)$$

$$\frac{k^\mu}{M_W} \tilde{T}_\mu^{hW}(k) = \tilde{T}^{hG} + \tilde{E}_R, \quad (4.17)$$

$$\frac{k^\mu}{M_W} T_\mu^{hW}(k) = T^{hG} + E_R, \quad (4.18)$$

$$\frac{k^\mu}{M_W} \tilde{T}_\mu^{Wh}(k) = -\tilde{T}^{Gh} - \tilde{E}_L, \quad (4.19)$$

where we have defined

$$E_L(p'_1, p'_2) = i \left(\frac{g_w}{\sqrt{2}} \right)^2 \frac{c_\beta}{M_W^2} \bar{u}_\mu(p'_2) B_{\mu\alpha}^R B_{e\alpha}^{L*} m_\alpha P_L v_e(p'_1), \quad (4.20)$$

$$\tilde{E}_R(p_1, p_2) = i \left(\frac{g_w}{\sqrt{2}} \right)^2 \frac{c_\beta}{M_W^2} \bar{v}_d(p_2) V_{id}^{L*} V_{is}^R m_i P_R u_s(p_1), \quad (4.21)$$

$$E_R(p'_1, p'_2) = i \left(\frac{g_w}{\sqrt{2}} \right)^2 \frac{c_\beta}{M_W^2} \bar{u}_\mu(p'_2) B_{\mu\alpha}^L B_{e\alpha}^{R*} m_\alpha P_R v_e(p'_1), \quad (4.22)$$

$$\tilde{E}_L(p_1, p_2) = i \left(\frac{g_w}{\sqrt{2}} \right)^2 \frac{c_\beta}{M_W^2} \bar{v}_d(p_2) V_{id}^{R*} V_{is}^L m_i P_R u_s(p_1). \quad (4.23)$$

With the help of the above Ward identities, the amplitude \mathcal{M}_a^ξ can then be rewritten as

$$\mathcal{M}_a^\xi = -\mathcal{M}_a^G + B_V^a + B_S^a, \quad (4.24)$$

where

$$B_V^a = \Delta_\xi(k) D_h(k') \left(T^{Gh} \tilde{E}_R + E_L \tilde{T}^{hG} \right), \quad (4.25)$$

$$B_S^a = \Delta_\xi(k) D_h(k') E_L \tilde{E}_R. \quad (4.26)$$

Following a similar procedure for the diagram 4(b), we obtain

$$\mathcal{M}_b^\xi = -\mathcal{M}_b^G + B_V^b + B_S^b. \quad (4.27)$$

The final expression for the box graphs 4(a) and 4(b) takes the form

$$\begin{aligned} \mathcal{M}_{\text{box}} &\equiv \mathcal{M}_a + \mathcal{M}_b \\ &= \mathcal{M}_a^U + \mathcal{M}_b^U + \mathcal{M}_a^\xi + \mathcal{M}_b^\xi + \mathcal{M}_a^G + \mathcal{M}_b^G \\ &= \mathcal{M}_{\text{box}}^U + B_V + B_S, \end{aligned} \quad (4.28)$$

where $\mathcal{M}_{\text{box}}^U = \mathcal{M}_a^U + \mathcal{M}_b^U$ is the contribution of the box diagrams evaluated in the unitary gauge, and

$$B_V = \Delta_\xi(k) D_h(k') \left(T^{Gh} \tilde{E}_R + E_L \tilde{T}^{hG} + T^{hG} \tilde{E}_L + E_R \tilde{T}^{Gh} \right), \quad (4.29)$$

$$B_S = \Delta_\xi(k) D_h(k') \left(E_L \tilde{E}_R + E_R \tilde{E}_L \right). \quad (4.30)$$

The presence of the terms B_V and B_S , which are proportional to the gauge-dependent propagator $\Delta_\xi(k)$, implies that the box diagrams in class C do not form a gauge-invariant set, and that additional vertex and self-energy graphs must be considered.

4.2 OSS renormalization of vertex diagrams

We now consider the contribution of the vertex diagrams 4(c)–(f) in the OSS renormalization scheme. After performing the $R1$ subtraction given in Eq. (4.1), we obtain the following matrix element for the vertex graphs:

$$\mathcal{M}_{\text{vertex}}^{R1} = \sum_{\varphi=\phi^{r,i}} \left[\Gamma_\varphi^0(p'_1, p'_2) \frac{i}{p^2 - M_\varphi^2} \tilde{\Gamma}_\varphi^{R1}(p^2) + \Gamma_\varphi^{R1}(p^2) \frac{i}{p^2 - M_\varphi^2} \tilde{\Gamma}_\varphi^0(p_1, p_2) \right], \quad (4.31)$$

where we have defined

$$\Gamma_{\phi_2^0}^0(p'_1, p'_2) = -\frac{M_W}{g_w c_\beta} E_S(p'_1, p'_2); \quad \Gamma_{\phi_2^0}^0(p'_1, p'_2) = -\frac{iM_W}{g_w c_\beta} E_P(p'_1, p'_2), \quad (4.32)$$

$$\tilde{\Gamma}_{\phi_2^0}^0(p_1, p_2) = -\frac{M_W}{g_w c_\beta} \tilde{E}_S(p_1, p_2); \quad \tilde{\Gamma}_{\phi_2^0}^0(p_1, p_2) = -\frac{iM_W}{g_w c_\beta} \tilde{E}_P(p_1, p_2), \quad (4.33)$$

with

$$E_{S,P}(p'_1, p'_2) = E_R(p'_1, p'_2) \pm E_L(p'_1, p'_2), \quad (4.34)$$

$$\tilde{E}_{S,P}(p_1, p_2) = \tilde{E}_R(p_1, p_2) \pm \tilde{E}_L(p_1, p_2). \quad (4.35)$$

The functions E_L , \tilde{E}_R , E_R , and \tilde{E}_L have previously been defined in Eqs. (4.20)–(4.23), respectively.

We now proceed by decomposing $\mathcal{M}_{\text{vertex}}^{R1}$ in terms of an $R1$ -subtracted amplitude in the unitary gauge and the remainder, *i.e.*,

$$\mathcal{M}_{\text{vertex}}^{R1} = \mathcal{M}_{\text{vertex}}^{U,R1} + V_S + V_B. \quad (4.36)$$

In analogy with Eqs. (4.7) and (4.8), the one-loop vertices involving the virtual states W_L and G_L may also be separated into two terms: $\Gamma_\varphi = \Gamma_\varphi^W + \Gamma_\varphi^G$ and for $\tilde{\Gamma}_\varphi$ likewise. Employing the identity

$$\Gamma_\varphi^{G,R1}(p^2) = \frac{p^2 - M_\varphi^2}{M_h^2 - M_\varphi^2} \Gamma_\varphi^G(p^2) - \left[\frac{p^2 - M_h^2}{M_h^2 - M_\varphi^2} \Gamma_\varphi^G(p^2) \right]^{R1}, \quad (4.37)$$

we can cast the different terms on the RHS of Eq. (4.36) into the form

$$\mathcal{M}_{\text{vertex}}^{U,R1} + V_S = \sum_{\varphi=\phi_2^{r,i}} \left\{ \Gamma_\varphi^0 \frac{i}{M_h^2 - M_\varphi^2} \left[\tilde{\Gamma}_\varphi^W(p^2) - \frac{p^2 - M_h^2}{M_h^2 - M_\varphi^2} \tilde{\Gamma}_\varphi^G(p^2) \right]^{R1} \right.$$

$$+ \left[\Gamma_\varphi^W(p^2) - \frac{p^2 - M_h^2}{M_h^2 - M_\varphi^2} \Gamma_\varphi^G(p^2) \right]^{R1} \frac{i}{p^2 - M_\varphi^2} \tilde{\Gamma}_\varphi^0 \}, \quad (4.38)$$

$$V_B = \sum_{\varphi=\phi_2^{r,i}} \left[\Gamma_\varphi^0 \frac{i}{M_h^2 - M_\varphi^2} \tilde{\Gamma}_\varphi^G(p^2) + \Gamma_\varphi^G(p^2) \frac{i}{M_h^2 - M_\varphi^2} \tilde{\Gamma}_\varphi^0 \right]. \quad (4.39)$$

Using the Feynman rules given in Appendix A, we can calculate the analytic expressions for the one-loop vertices. These are given by

$$\Gamma_{\phi_2^r}^G(p^2) = -\frac{ig_w c_\beta}{2M_W} (M_h^2 - M_{\phi_2^r}^2) \Delta_\xi(k) D_h(k') (T^{hG} + T^{Gh}), \quad (4.40)$$

$$\Gamma_{\phi_2^i}^G(p^2) = \frac{g_w c_\beta}{2M_W} (M_h^2 - M_{\phi_2^i}^2) \Delta_\xi(k) D_h(k') (T^{hG} - T^{Gh}), \quad (4.41)$$

$$\tilde{\Gamma}_{\phi_2^r}^G(p^2) = -\frac{ig_w c_\beta}{2M_W} (M_h^2 - M_{\phi_2^r}^2) \Delta_\xi(k) D_h(k') (\tilde{T}^{hG} + \tilde{T}^{Gh}), \quad (4.42)$$

$$\tilde{\Gamma}_{\phi_2^i}^G(p^2) = \frac{g_w c_\beta}{2M_W} (M_h^2 - M_{\phi_2^i}^2) \Delta_\xi(k) D_h(k') (\tilde{T}^{hG} - \tilde{T}^{Gh}), \quad (4.43)$$

$$\Gamma_{\phi_2^r}^W(p^2) = \frac{ig_w c_\beta}{2} (M_h^2 - M_{\phi_2^r}^2) \left[U^{\mu\nu}(k) - \frac{k^\mu k^\nu}{M_W^2} \Delta_\xi(k) \right] D_h(k') (T_\nu^{hW} - T_\nu^{Wh}) (k' + p)_\mu, \quad (4.44)$$

$$\Gamma_{\phi_2^i}^W(p^2) = -\frac{g_w c_\beta}{2} (M_h^2 - M_{\phi_2^i}^2) \left[U^{\mu\nu}(k) - \frac{k^\mu k^\nu}{M_W^2} \Delta_\xi(k) \right] D_h(k') (T_\nu^{hW} + T_\nu^{Wh}) (k' + p)_\mu, \quad (4.45)$$

$$\tilde{\Gamma}_{\phi_2^r}^G(p^2) = \frac{ig_w c_\beta}{2} (M_h^2 - M_{\phi_2^r}^2) \left[U^{\mu\nu}(k) - \frac{k^\mu k^\nu}{M_W^2} \Delta_\xi(k) \right] D_h(k') (\tilde{T}_\nu^{Wh} - \tilde{T}_\nu^{hW}) (k' + p)_\mu, \quad (4.46)$$

$$\tilde{\Gamma}_{\phi_2^i}^G(p^2) = -\frac{g_w c_\beta}{2} (M_h^2 - M_{\phi_2^i}^2) \left[U^{\mu\nu}(k) - \frac{k^\mu k^\nu}{M_W^2} \Delta_\xi(k) \right] D_h(k') (\tilde{T}_\nu^{hW} + \tilde{T}_\nu^{Wh}) (k' + p)_\mu. \quad (4.47)$$

With the help of these expressions, it is now straightforward to show that

$$V_B = -B_V. \quad (4.48)$$

Evidently, in the evaluation of the total matrix element, V_B will cancel against the ξ -dependent term B_V coming from the box diagrams (*cf.* (4.29)).

We will now determine the analytic form of the ξ -dependent term V_S in Eq. (4.38). For this purpose, it is useful to introduce the abbreviation

$$\bar{\Gamma}_\varphi(p^2) \equiv \Gamma_\varphi^W(p^2) - \frac{p^2 - M_h^2}{M_h^2 - M_\varphi^2} \Gamma_\varphi^G(p^2). \quad (4.49)$$

We can now express $\bar{\Gamma}_{\phi_2^r}(p^2)$ as follows:

$$\begin{aligned} \bar{\Gamma}_{\phi_2^r}(p^2) &= \Gamma_{\phi_2^r}^U(p^2) - \frac{ig_w c_\beta}{2M_W} (T^{hG} + T^{Gh}) \Delta_\xi(k) + \frac{ig_w c_\beta}{2M_W} E_S \Delta_\xi(k) \\ &\quad - \frac{ig_w c_\beta}{2M_W} (p^2 - M_h^2) E_S \Delta_\xi(k) D_h(k'). \end{aligned} \quad (4.50)$$

Here, $\Gamma_{\phi_2^r}^U(p^2)$ denotes the one-loop $\phi_2^r \mu^- e^+$ coupling, evaluated in the unitary gauge. Since the second and the third term vanish under the $R1$ operation, as they do not depend on p^2 , we then obtain for the OSS renormalized vertex function

$$\bar{\Gamma}_{\phi_2^r}^{R1}(p^2) = \Gamma_{\phi_2^r}^{U,R1}(p^2) - \frac{ig_w c_\beta}{2M_W} E_S \left[(p^2 - M_h^2) \Delta_\xi(k) D_h(k') \right]^{R1}. \quad (4.51)$$

The first term on the RHS of Eq. (4.51) is needed to obtain $\mathcal{M}_{\text{vertex}}^{U,R1}$ in Eq. (4.38), whereas the remainder is a function that depends on ξ explicitly. Including both ϕ_2^r and ϕ_2^i contributions, we obtain the ξ -dependent function V_S

$$V_S = - \left[(p^2 - M_h^2) \Delta_\xi(k) D_h(k') \right]^{R1} \left(E_S \tilde{E}_S \frac{1}{p^2 - M_{\phi_2^r}^2} - E_P \tilde{E}_P \frac{1}{p^2 - M_{\phi_2^i}^2} \right). \quad (4.52)$$

In the following, we shall show how the ξ -dependent terms V_S and B_S , defined in Eqs. (4.52) and (4.30), respectively, will cancel against corresponding ξ -dependent terms coming from the self-energy graphs, shown in Figs. 4(g) and 4(h).

4.3 OSS renormalization of self-energy diagrams

We shall now calculate the amplitude related to the self-energy graphs (g)–(h) in Fig. 4. After carrying the $R2$ subtraction defined in Eq. (4.2), we may conveniently write the self-energy-like amplitude as

$$\mathcal{M}_{\text{self}}^{R2} = - \sum_{\varphi=\phi_2^{r,i}} \Gamma_\varphi^0 \frac{1}{p^2 - M_\varphi^2} \Pi_\varphi^{R2}(p^2) \frac{1}{p^2 - M_\varphi^2} \tilde{\Gamma}_\varphi^0. \quad (4.53)$$

By analogy, we also write the self-energy of the FCNC scalars as a sum of two terms:

$$\Pi_\varphi(p^2) = \Pi_\varphi^W(p^2) + \Pi_\varphi^G(p^2), \quad (4.54)$$

where $\Pi_\varphi^W(p^2)$ and $\Pi_\varphi^G(p^2)$ are respectively the graphs with W_L and G_L bosons in the loop. The action of $R2$ operation on the self-energy $\Pi_\varphi^G(p^2)$ gives

$$\begin{aligned} \Pi_\varphi^{G,R2}(p^2) &= \left(\frac{p^2 - M_\varphi^2}{M_h^2 - M_\varphi^2} \right)^2 \Pi_\varphi^G(p^2) - 2 \frac{p^2 - M_\varphi^2}{(M_h^2 - M_\varphi^2)^2} \left[(p^2 - M_h^2) \Pi_\varphi^G(p^2) \right]^{R1} \\ &+ \left[\left(\frac{p^2 - M_h^2}{M_h^2 - M_\varphi^2} \right) \Pi_\varphi^G(p^2) \right]^{R2}. \end{aligned} \quad (4.55)$$

With the help of Eq. (4.55), the self-energy-like amplitude may be decomposed as follows:

$$\mathcal{M}_{\text{self}}^{R2} = \mathcal{M}_{\text{self}}^{U,R2} + S_B + S_V, \quad (4.56)$$

where

$$\mathcal{M}_{\text{self}}^{U,R2} = - \sum_{\varphi=\phi_2^{r,i}} \Gamma_\varphi^0 \left[\left(\frac{p^2 - M_h^2}{M_h^2 - M_\varphi^2} \right) \Pi_\varphi^G(p^2) + \Pi_\varphi^W(p^2) \right]^{R2} \tilde{\Gamma}_\varphi^0, \quad (4.57)$$

$$S_B = - \sum_{\varphi=\phi_2^{r,i}} \Gamma_\varphi^0 \frac{1}{(M_h^2 - M_\varphi^2)^2} \Pi_\varphi^G(p^2) \tilde{\Gamma}_\varphi^0, \quad (4.58)$$

$$S_V = \sum_{\varphi=\phi_2^{r,i}} \Gamma_\varphi^0 \frac{2}{(M_h^2 - M_\varphi^2)(p^2 - M_\varphi^2)} \left[(p^2 - M_h^2) \Pi_\varphi^G(p^2) \right]^{R1} \tilde{\Gamma}_\varphi^0. \quad (4.59)$$

We should now show that $\mathcal{M}_{\text{self}}^{U,R2}$ in Eq. (4.57) is indeed the OSS renormalized self-energy-like amplitude in the unitary gauge. To make this explicit, we first calculate the analytic expressions for all the scalar self-energies $\Pi_\varphi^W(p^2)$ and $\Pi_\varphi^G(p^2)$ before applying the $R2$ subtraction. Using the Feynman rules listed in Appendix A and omitting loop integration, the different self-energy contributions read:

$$\Pi_{\phi_2^r}^G(p^2) = \frac{2c_\beta^2}{M_W^2} \left(\frac{g_w}{2} \right)^2 (M_h^2 - M_{\phi_2^r}^2)^2 \Delta_\xi(k) D_h(k'), \quad (4.60)$$

$$\Pi_{\phi_2^i}^G(p^2) = \frac{2c_\beta^2}{M_W^2} \left(\frac{g_w}{2} \right)^2 (M_h^2 - M_{\phi_2^i}^2)^2 \Delta_\xi(k) D_h(k'), \quad (4.61)$$

$$\Pi_{\phi_2^r}^W(p^2) = 2c_\beta^2 \left(\frac{g_w}{2} \right)^2 \left[U_{\mu\nu}(k) - \frac{k_\mu k_\nu}{M_W^2} \Delta_\xi(k) \right] D_h(k') (p + k')^\mu (p + k')^\nu, \quad (4.62)$$

$$\Pi_{\phi_2^i}^W(p^2) = \Pi_{\phi_2^r}^W(p^2). \quad (4.63)$$

Taking these last results into account, we obtain for the expression within the square brackets, which appears on the RHS of Eq. (4.57),

$$\begin{aligned} & \left(\frac{p^2 - M_h^2}{M_h^2 - M_{\phi_2^r}^2} \right) \Pi_{\phi_2^r}^G(p^2) + \Pi_{\phi_2^r}^W(p^2) \\ &= \Pi_{\phi_2^r}^U(p^2) - \frac{2c_\beta^2}{M_W^2} \left(\frac{g_w}{2} \right)^2 \left[2(p^2 - M_h^2) - (k'^2 - M_h^2) \right] \Delta_\xi(k). \end{aligned} \quad (4.64)$$

The first term in Eq. (4.64) is the ϕ_2^r self-energy in the unitary gauge, whereas the second term, being only linear in p^2 , will vanish after the $R2$ operation, which requires two subtractions. As a result, $\mathcal{M}_{\text{self}}^{U,R2}$ is indeed the OSS-renormalized self-energy-like amplitude in the unitary gauge.

We are then left with the gauge-dependent terms S_B and S_V , which can be conveniently re-expressed as follows:

$$S_B = -\Delta_\xi(k) D_h(k') (E_R \tilde{E}_L + E_L \tilde{E}_R), \quad (4.65)$$

$$S_V = \left[(p^2 - M_h^2) \Delta_\xi(k) D_h(k') \right]^{R1} \left(E_S \tilde{E}_S \frac{1}{p^2 - M_{\phi_2^r}^2} - E_P \tilde{E}_P \frac{1}{p^2 - M_{\phi_2^i}^2} \right). \quad (4.66)$$

By simple comparison of Eqs. (4.65) and (4.66) with Eqs. (4.30) and (4.52), it is easy to see that

$$S_B = -B_S, \quad S_V = -V_S \quad (4.67)$$

This very last result concludes our proof of gauge-invariance of the diagrams in group C, presented in Fig. 4.

To sum up, we have shown that the total amplitude \mathcal{M} of the diagrams shown in Fig. 4 is ξ independent in the OSS renormalization scheme. As it should, \mathcal{M} equals the result obtained in the unitary gauge, *i.e.*,

$$\begin{aligned} \mathcal{M} &= \mathcal{M}_{\text{box}} + \mathcal{M}_{\text{vertex}}^{R1} + \mathcal{M}_{\text{self}}^{R2} \\ &= \mathcal{M}_{\text{box}}^U + \mathcal{M}_{\text{vertex}}^{U,R1} + \mathcal{M}_{\text{self}}^{U,R2}. \end{aligned} \quad (4.68)$$

In particular, we have seen how the gauge-dependent terms originating from the box graphs cancel against self-energy and the vertex contributions after OSS renormalization. A line of similar steps may be followed to show the gauge independence of the group B. Therefore, expressions analogous to Eq. (4.68) are to be used in our phenomenological considerations in Section 5.

5 Discussion and numerical results

The branching ratio $B(K_L \rightarrow e\mu)$ given in Eq. (3.6) depends on the reduced amplitudes \mathcal{A} and \mathcal{B} , which in turn depend on many kinematic parameters. Since our analytic results are shown to be gauge independent in Section 4, we shall henceforth adopt the Feynman-'t Hooft gauge in the discussion that follows. First, we will qualitatively estimate the dominant one-loop contributions to the chirality enhanced amplitude \mathcal{B} . Then, we will compare these estimates with those obtained for the $K^0\bar{K}^0$ system and underline the crucial difference of the one-loop results for $K_L \rightarrow e\mu$ with those found for the $K^0\bar{K}^0$ system. In addition, we will point out the main improvements of our analysis, compared to earlier studies. Using the complete analytic expressions listed in Appendix B, we will present numerical predictions for $B(K_L \rightarrow e\mu)$ in manifest and non-manifest left-right models and determine the allowed parameter space, when the experimental limit B_{exp} in Eq. (1.1) is implemented.

We shall now discuss the qualitative behaviour of the individual contributions to the decay amplitude $\mathcal{T}(\bar{K}^0 \rightarrow e^+\mu^-)$ in the limit $m_{N_1}, m_{N_2} \gg M_R \gg M_W$. In this heavy-neutrino limit, the reduced amplitude, \mathcal{A}_{LL} , which describes the contribution from the two

W_L bosons in the loop, behaves as

$$\mathcal{A}_{LL} \approx \frac{1}{4} V_{td}^{L*} V_{ts}^L \frac{m_D^2}{m_M^2} \frac{m_t^2}{M_W^2} \ln \left(\frac{m_N^2}{m_t^2} \right). \quad (5.1)$$

In deriving Eq. (5.1), we have used the approximation: $s_L^{\nu_i} m_N \approx m_D$. We see that \mathcal{A}_{LL} decreases in magnitude for large m_M values when m_D is kept fixed, whereas the Dirac masses m_D do not decouple for fixed values of m_M . Precisely the existence of this non-decoupling window due to high Dirac masses m_D has led to enhanced predictions for lepton-flavour- and universality-violating processes in minimal extensions of the SM with right-handed neutrinos [13,15,16,17]. For ultra-heavy neutrinos, the reduced amplitude \mathcal{A}_{RR} originating from two W_R bosons shows up a behaviour quite analogous to \mathcal{A}_{LL} , *i.e.*,

$$\mathcal{A}_{RR} \approx \frac{1}{4} V_{td}^{R*} V_{ts}^R \frac{m_D^2}{m_M^2} \frac{m_t^2}{M_R^2} \ln \left(\frac{m_N^2}{m_t^2} \right). \quad (5.2)$$

In analogy to \mathcal{A}_{LL} , \mathcal{A}_{RR} vanishes when $m_M \rightarrow \infty$.

As has already been noticed in [10], the dominant one-loop contribution to $\mathcal{T}(\bar{K}^0 \rightarrow e^+ \mu^-)$ comes from the box graphs with virtual Goldstone bosons G_L^+ and G_R^+ in Figs. 3(a) and 3(b). In Section 4 we have seen however that the box graphs are not gauge independent by themselves, and it is therefore important to include the respective gauge-dependent complements originating from graphs in Figs. 3(g) and 3(h). If these additional contributions are included, we observe that the gauge-independent reduced amplitude $\eta \mathcal{B}$ is still chirality enhanced due to the simultaneous presence of left- and right-handed currents in the loop. Expanding to leading order in the large parameters $\beta \lambda_N = m_N^2/M_R^2$ (with $\beta = M_W^2/M_R^2$) and $\lambda_t = m_t^2/M_W^2$, we find

$$\begin{aligned} \eta \mathcal{B}(3a + 3b + 3g + 3h) &\approx \eta (V_{td}^{L*} V_{ts}^R B_{\mu N}^R B_{eN}^{L*} + V_{td}^{R*} V_{ts}^L B_{\mu N}^L B_{eN}^{R*}) \beta (\lambda_t \lambda_N)^{1/2} \\ &\quad \times \left(1 + \beta \lambda_t \ln \beta + \frac{\beta \lambda_t^2 \ln \lambda_t}{\lambda_t - 1} \right) \\ &\approx \eta (V_{td}^{L*} V_{ts}^R + V_{td}^{R*} V_{ts}^L) \frac{m_t m_D}{M_R^2}. \end{aligned} \quad (5.3)$$

In the last approximate equality of Eq. (5.3), we have used again the fact that $s_L^{\nu_i} m_N \approx m_D$ and $\beta \ll 1$. In contrast to \mathcal{A}_{LL} and \mathcal{A}_{RR} , $\eta \mathcal{B}$ does not vanish in the $m_M/v_R \rightarrow \infty$. This is a novel consequence of the left-right models and cannot occur in other models, in which gauge interactions conserve chirality, such as $SU(2)_L \otimes U(1)_Y$ scenarios with right-handed neutrinos [26].

Apart from restoration of gauge independence, it should be stressed again that the one-loop self-energies of the FCNC Higgs scalars play a very crucial rôle in the phenomenology of $K_L \rightarrow e\mu$. In the Feynman-'t Hooft gauge, the dominant contribution to the reduced

amplitude \mathcal{B} is due the Higgs self-energies in Figs. 3(g) and 3(h). Their contribution relative to the box diagrams may be determined from the ratio

$$r_{\text{box/FCNC}} \equiv \frac{\mathcal{B}(3a + 3b)}{\mathcal{B}(3g + 3h)} \approx \frac{\beta\lambda_t \ln \beta + 8 \ln \beta/\lambda_N}{-1 + \frac{1}{2} \ln(M_\phi^2/M_R^2)}. \quad (5.4)$$

We see that the contribution of the FCNC Higgs self-energies to $\mathcal{T}(\bar{K}^0 \rightarrow e^+\mu^-)$ is considerably enhanced by a factor $\sim 1/\beta$ in comparison with that of the box diagrams. From Eq. (5.4), we can readily deduce that $r_{\text{box/FCNC}} \leq 1$, unless $\beta \leq 0.01$ and $m_N \leq 1$ TeV. However, for the parameter range, in which the box graphs are dominant, we find that the branching ratio is at least by one order of magnitude smaller than the present experimental limit B_{exp} given in Eq. (1.1).

In the manifest left-right symmetric model (LRSM) (*i.e.*, $V^L = V^R = V$), the chirality enhanced amplitude $\eta\mathcal{B}$ in Eq. (5.3) can lead to a combined constraint on m_D and M_R , when the experimental limit on $K_L \rightarrow e\mu$ is considered. In particular, we find the inequality

$$\frac{m_t m_D}{M_R^2} \lesssim 4. \times 10^{-3}. \quad (5.5)$$

If we assume the lowest W_R -boson mass allowed from $K^0\bar{K}^0$ mixing [35,36], *i.e.*, $M_R = 1.5$ TeV, this then leads to $m_D < 45$ GeV. This bound becomes much weaker for heavy W_R bosons, *e.g.*, $m_D < 0.5$ TeV for $M_R = 5$ TeV.

In the manifest LRSM, the largest effect in the decay amplitude due to the box graphs comes from the top quark, whereas charm-quark effects are in general sub-dominant. The relative behaviour of the charm- to top-quark contribution is given by the ratio

$$r_{c/t}^{\text{box}} \approx \frac{m_c V_{cd}^* V_{cs}}{m_t V_{td}^* V_{ts}} \frac{4}{4 + \beta\lambda_t\lambda_N} \approx \frac{8}{4 + \beta\lambda_t\lambda_N}. \quad (5.6)$$

From Eq. (5.6), we see that top-quark mass effects dominate over the charm-quark effects in the box diagrams, when $m_N \gg M_R$. The situation is very different for the $K^0\bar{K}^0$ mixing, in which charm-quark yields the most dominant contribution in the loop [19]. The reason for this crucial difference is that the one-loop box functions show up an enhanced behaviour, when the largest fermionic mass in the loop is much bigger than M_R . Obviously, in $K^0\bar{K}^0$ mixing, the highest fermionic mass scale is set up by the top quark, which is much smaller than the W_R -boson mass, whereas the heavy neutrinos can be much heavier than W_R in the decay amplitude for $K_L \rightarrow e\mu$. In the manifest LRSM, we can estimate the relative contribution of the one-loop box functions for the two cases mentioned above as follows:

$$\frac{\mathcal{A}_{\text{box}}(K^0 - \bar{K}^0)}{\mathcal{B}_{\text{box}}(K_L \rightarrow e\mu)} \approx \frac{V_{cd}^* V_{cs}}{(s_L^{\nu_e}) \beta\lambda_t^{1/2} \lambda_N^{1/2}}. \quad (5.7)$$

This discussion shows how heavy Majorana neutrinos with masses $m_N \gg M_R$ are phenomenologically very significant for enhancing the decay rate of $K_L \rightarrow e\mu$.

The decay $K_L \rightarrow e\mu$ can also proceed via a tree-level FCNC Higgs exchange. Therefore, it is most important to compare the FCNC self-energy contribution with that of the tree-level amplitude. In particular, we find the ratio

$$\frac{\mathcal{B}_{\text{tree}}}{\mathcal{B}(3g + 3h)} \approx \frac{4\pi M_R^2}{\alpha_w \mathcal{O}(1) M_\phi^2} \approx (190 - 380) \times \frac{M_R^2}{M_\phi^2}. \quad (5.8)$$

It is easy to see that $\mathcal{B}(3g + 3h)$ is getting larger than $\mathcal{B}_{\text{tree}}$ for $M_\phi \gtrsim 15M_R$. On the other hand, the constraint that theory should remain perturbative at high energies gives rise to the unitarity bound in Eq. (3.10). As opposed to $K^0 \bar{K}^0$ mixing, the tree-level Higgs contributions to the decay $K_L \rightarrow e\mu$ are always comparable to the one-loop effects, and hence both must be included in the analysis. This constitutes another non-trivial feature for the decay $K_L \rightarrow e\mu$, which is to be examined carefully in the numerical estimates.

In the numerical estimates, we consider two representative variants of left-right models: (i) the manifest or pseudo-manifest LRSM (*i.e.* $V^L = V^R = V$), in which the Dirac mass matrix m_D is still different from the charged-lepton mass matrix M_l , and (ii) the non-manifest LRSM, where $V^L = V$ but $V^R \neq V$. Implementing the results of Ref. [22], we choose natural relations and mass hierarchies among the kinematic parameters of the left-right models. In particular, we set all heavy Higgs particles to be degenerate, *i.e.*, $M_{\phi_2^r} = M_{\phi_2^i} = M_\phi$ and $M_h = M_\phi$ (*cf.* Eq. (2.6)). Already a small mass difference between the FCNC Higgs scalars would be sufficient to induce a large negative radiative shift in $R_b = \Gamma(Z \rightarrow b\bar{b})/\Gamma(Z \rightarrow \text{hadrons})$, which would be incompatible with the existing tight constraints on this LEP observable [17].

To reduce even further the number of the many free parameters, we fix $(s_L^{\nu e})^2 = 10^{-4}$, $(s_L^{\nu\mu})^2 = 0$ and the angle $\theta_R = \pi/4$ in Eq. (2.20). This choice of heavy-light neutrino mixings is in compliance with other low-energy constraints derived in Eqs. (2.24) and (2.25). For simplicity, we also assume that the two heavy neutrinos, N_1 and N_2 , have the same mass, *i.e.*, $m_{N_1} = m_{N_2} = m_N$, and the heavy neutrino mass m_N is varied from 100 GeV up to the perturbative unitarity limit 50 TeV [26], which is compatible with the limit of Eq. (2.26). The input values for the entries of the CKM matrix $V = V^L$ are [1]: $V_{cd} = 0.224$, $V_{cs} = 0.975$, $V_{td} = 0.015$ and $V_{ts} = 0.048$. In the non-manifest LRSM, the mixing matrix V^R for the right-handed quarks is in general arbitrary and is only subject to phenomenological constraints. Here, we set $V_{cd}^R = V_{ts}^R = 1$ and $V_{cs}^R = V_{td}^R = 0$, which leads to an enhanced charm-quark contribution to the decay amplitude, and in this respect, this model differs from the manifest LRSM.

Since we are interested in investigating the individual tree and one-loop contributions to the decay amplitude $\mathcal{T}(\bar{K}^0 \rightarrow e^+\mu^-)$, our numerical estimates for $B(K_L \rightarrow e\mu)$ are computed from the four different squared matrix elements:

$$\begin{aligned}
\text{I.} & \quad |\mathcal{T}_{\text{tree}}|^2 \quad (\text{solid}), \\
\text{II.} & \quad |\mathcal{T}_{\text{tree}}|^2 + 2\Re(\mathcal{T}_{\text{tree}}\mathcal{T}_{1\text{-loop}}^*) \quad (\text{dashed}), \\
\text{III.} & \quad |\mathcal{T}_{1\text{-loop}}|^2 \quad (\text{dotted}), \\
\text{IV.} & \quad |\mathcal{T}_{\text{tree}} + \mathcal{T}_{1\text{-loop}}|^2 \quad (\text{dash-dotted}).
\end{aligned} \tag{5.9}$$

In Eq. (5.9), the type of lines used in the plots for the four different predictions is specified within the parentheses. The results obtained from the expressions I and II are those that are based on a consistent loop expansion of the squared decay amplitude $|\mathcal{T}(\bar{K}^0 \rightarrow e^+\mu^-)|^2$. For comparison, we also give numerical estimates derived from the formulae III and IV.

In Fig. 7, we display the dependence of $B(K_L \rightarrow e\mu)$ on the heavy Majorana mass m_N for the selected values of the W_R -boson mass $M_R = 1, 2, 5$ and 10 TeV in the manifest LRSM. In agreement with Eq. (5.3), we find a strong dependence of $B(K_L \rightarrow e\mu)$ on m_N^2 . This non-decoupling behaviour of the heavy neutrinos enters via the Dirac mass terms m_D of the see-saw type mass matrix in Eq. (2.9) [17]. We see that the pure one-loop contributions to the squared decay amplitude (dotted line) are always comparable to the respective tree-level results (solid line). In the manifest LRSM, the W_R -boson mass is severely constrained by the experimental limit on the $K^0\bar{K}^0$ mixing. After including QCD corrections, the authors in [35] find $M_R \gtrsim 2.5$ TeV in the limit of very large FCNC Higgs masses. In all plots in Fig. 7, we take $M_\phi = 15M_R$, for definiteness. As can be seen from Fig. 7(c), for example, for sufficiently heavy Majorana neutrinos, $B(K_L \rightarrow e\mu)$ may exceed the present experimental bound, which is indicated by an horizontal dotted line in all plots. Thus, for $M_R \approx 2.5$ TeV, we find that $m_N \lesssim 10$ TeV, for the set of the input parameters mentioned above.

Fig. 8 gives the numerical predictions obtained in the non-manifest LRSM. We use the same input parameters as those of Fig. 7, except of the fact that we now consider the afore-mentioned V^R matrix, which significantly suppresses the top-quark contribution in the loop. In this scenario, the chirality mass enhancement due to the heavy top quark is no longer applicable and pure loop-effects (dotted line) on $K_L \rightarrow e\mu$ are at most 10% in comparison to the tree-level results for the experimentally accessible region. In fact, the tree-level effects on $K_L \rightarrow e\mu$ are more significant than the manifest LRSM case. The latter leads to tighter constraints on the heavy Majorana mass m_N . It is interesting to note that the non-manifest LRSM at hand does not invalidate the experimental bound due to $K^0\bar{K}^0$ mixing. As a result, even relatively light heavy Majorana neutrinos with masses of few hundreds of GeV can account for possible lepton-flavour violating decays of K_L .

In Figs. 9 and 10, we examine the dependence of $B(K_L \rightarrow e\mu)$ as a function of M_R in the manifest and non-manifest LRSM, respectively. We vary the W_R -boson mass from 0.5 to 20 TeV, for different values of the heavy neutrino mass m_N . The FCNC Higgs scalar mass M_ϕ is also varied in linear dependence of M_R , as is explicitly shown in the plots. As is expected, we observe the generic feature of decoupling of a very large W_R mass from the theory. In the manifest LRSM (see Fig. 9), $B(K_L \rightarrow e\mu)$ is difficult to measure for $M_R > 7$ TeV, even if rather heavy Majorana neutrinos and FCNC Higgs bosons are assumed. In the case of non-manifest LRSM, the respective mass bound is slightly weaker, *i.e.*, $M_R > 10$ TeV, as can be seen from Fig. 10.

It is now interesting to investigate the impact of both the FCNC Higgs-scalar and W_R -boson masses on $B(K_L \rightarrow e\mu)$. To this end, we present exclusion plots in Figs. 11 and 12 for the manifest and non-manifest LRSM, respectively. The allowed areas in the M_ϕ - M_R plane are determined from the inequality $B(K_L \rightarrow e\mu) < B_{\text{exp}}$, where $B(K_L \rightarrow e\mu)$ has been calculated using the squared matrix elements in Eq. (5.9) for different values of the heavy neutrino mass. The solid, dotted and dashed lines exclude the areas, in which the ‘ m_N ’ label is not contained. Clearly, the tree-level results (solid line) are independent of the W_R mass, and are in qualitative agreement with Eq. (3.9). In contrast, the results derived from the one-loop expression III in Eq. (5.9) (dotted line) are insensitive to variations of M_ϕ . We include the constraints obtained from the squared matrix element III, since they will become significant beyond one loop. The dashed lines represent the limits obtained from the expression II in Eq. (5.9), whereas results based on the squared matrix element IV are not shown. To a good approximation, the latter may be represented equally well by the combined graphical effect of all the three lines mentioned above. From Figs. 11 and 12, we can see that a large region of the parameter space of the two typical LRSM’s can be excluded by the experimental limit on the decay $K_L \rightarrow e\mu$. For the values of the light-heavy neutrino mixings $(s_L^{\nu e})^2 = 10^{-4}$, $(s_L^{\nu \mu})^2 = 0$, a relatively low W_R mass, *i.e.*, $M_R < 1$ TeV, cannot naturally accommodate the experimental data from $K_L \rightarrow e\mu$ and $K^0\bar{K}^0$ mixing, without recourse to excessive fine tuning in the parameter space of the left-right models.

6 Conclusions

We have studied the lepton-flavour-violating decay $K_L \rightarrow e\mu$ within the framework of $SU(2)_R \otimes SU(2)_L \otimes U(1)_{(B-L)}$ models. Experiments searching for this decay mode are very important, since they can offer complementary limits on the parameter space of the left-right models together with limits obtained from the absence of $\mu \rightarrow e\gamma$, $\mu - e$ conversion in nuclei and $\mu \rightarrow eee$, and from the observed $K_L K_S$ mass difference.

We have seen that one-loop box diagrams are not sufficient to provide a gauge-invariant result. Working in the R_ξ gauges and adopting the well-defined OSS renormalization, we have shown explicitly how gauge independence is restored in the transition amplitude, $\mathcal{T}(\bar{K}^0 \rightarrow e^+\mu^-)$, at one loop, when the corresponding self-energy and vertex graphs involving the FCNC Higgs scalars are taken into account. In fact, in the Feynman–’t Hooft gauge, the gauge-dependent complements of the box graphs may become dominant for a large range of the parameters. This novel aspect has not been addressed in detail in the existing literature before.

Using gauge-independent analytic expressions for the one-loop matrix element, we have performed a systematic analysis studying the explicit dependence of $B(K_L \rightarrow e\mu)$ on the various kinematic parameters. If we keep the enhanced light-heavy neutrino mixing $s_L^{\nu_i} \sim m_D/m_M$ fixed and increase the high Dirac mass terms in the left-right model, which arise from the spontaneous breakdown of the $SU(2)_L$ gauge symmetry, we obtain a quadratic dependence of the one-loop transition amplitude on the heavy neutrino mass. In contrast, if we hold m_D fixed below the perturbative unitarity bound but vary the Majorana mass scale m_M , then the transition amplitude arising from the left-handed currents, *e.g.*, from two W_L^+ bosons, vanishes in the limit $m_M \rightarrow \infty$, namely, $\mathcal{A}_{LL} \rightarrow 0$. As is expected on theoretical grounds, heavy neutrinos being singlets under $SU(2)_L$ will eventually decouple in this limit. Of course, these are known facts that have already been observed in [13] and subsequently discussed in many articles [14,15,16,17]. Finally, our numerical estimates confirm the non-decoupling behaviour of the heavy neutrinos due to high $SU(2)_L$ Dirac mass terms.

In LRSM’s with enhanced light-heavy neutrino mixing, however, there exists an additional heavy-neutrino enhancement due to the simultaneous presence of left- and right-handed currents in the loop [10]. These chirality-changing currents give rise to the reduced amplitude \mathcal{B} in the decay amplitude (3.1). Since m_M is not a iso-singlet mass term under $SU(2)_R$, we have found that \mathcal{B} tends to the non-vanishing expression $m_t m_D / M_R^2$ in Eq. (5.3) for $m_M \rightarrow \infty$ and fixed VEV v_R . Clearly, m_M/v_R cannot be arbitrarily large but should satisfy the perturbative bound (2.27). It may be worth emphasizing again that the observed non-decoupling behaviour of heavy neutrinos in the reduced amplitude \mathcal{B} is a novelty in the left-right models and has no analogue in the SM with right-handed neutrinos discussed above. In fact, we have found that the new non-decoupling phenomenon can only originate from amplitudes, which violate chirality in the loop, thereby allowing for an active interplay between the left-handed mass scale m_D and the right-handed one m_M .

Numerical estimates have shown that a significant part of the parameter space of the left-right models may be constrained due to the dominant contribution of \mathcal{B} and other low-

energy data. Since these constraints depend in general on many independent parameters, we have systematized the presentation of our results in a number of plots in Figs. 7 – 12. In the numerical estimates we have studied the manifest as well as a typical non-manifest left-right model. To exemplify further the significance of such an analysis, we note in passing that for $m_N \approx 10$ TeV, $s_L^{\nu e} \approx 10^{-2}$ and very heavy FCNC Higgs scalars, exclusion plots lead to W_R boson that must be heavier than about 3 TeV in the manifest left-right symmetric models (*cf.* Fig. 11(d)).

In conclusion, if experiments at DAΦNE or other future machines could substantiate a non-vanishing $B(K_L \rightarrow e\mu)$ at the level of $10^{-11} - 10^{-12}$, this would be naturally accounted for within left-right models through the novel non-decoupling behaviour of the heavy neutrinos in the chirality-changing amplitudes. In the manifest left-right symmetric models, such an explanation would require relatively light W_R -boson masses with $M_R \approx 2$ TeV and heavy neutrinos of several TeV, for light-heavy neutrino mixings $s_L^{\nu e} \approx 10^{-2}$, constraints which are in compliance with all other low-energy data.

Acknowledgements. K.S. would like to thank Ben Grinstein and the UCSD physics department for their hospitality. The work of K.S. is supported in part by the Volkswagen-Stiftung.

A Feynman rules in the LRSM

In this appendix, we list all the relevant Feynman rules obtained within the left-right models, which govern the interactions of the gauge and Higgs bosons with leptons and quarks, as well as the trilinear self-couplings of the bosons. In particular, we assume that the $SU(2)_L$ weak coupling constant g_L is equal to the corresponding $SU(2)_R$ one g_R , *i.e.*, $g_L = g_R$.

With the assumptions and simplifications mentioned above, the trilinear couplings among gauge, Higgs, and would-be Goldstone bosons, which are only relevant for $K_L \rightarrow e\mu$, are given by (all momenta flow into the vertex)

$$W_R^{\mp\mu}(p)\phi_2^r(q)W_L^{\pm\nu}(r) : \quad -ig_w M_W g_{\mu\nu}, \quad (\text{A.1})$$

$$W_R^{\mp\mu}(p)\phi_2^i(q)W_L^{\pm\nu}(r) : \quad \pm g_w M_W g_{\mu\nu}, \quad (\text{A.2})$$

$$G_R^\pm(p)\phi_2^r(q)W_L^{\mp\mu}(r) : \quad \mp i \frac{g_w}{2} s_\beta (p-q)_\mu, \quad (\text{A.3})$$

$$G_R^\pm(p)\phi_2^i(q)W_L^{\mp\mu}(r) : \quad -\frac{g_w}{2} s_\beta (p-q)_\mu, \quad (\text{A.4})$$

$$G_L^\pm(p)\phi_2^r(q)W_R^{\mp\mu}(r) : \quad \mp i \frac{g_w}{2} (p-q)_\mu, \quad (\text{A.5})$$

$$G_L^\pm(p)\phi_2^i(q)W_R^{\mp\mu}(r) : \quad \frac{g_w}{2} (p-q)_\mu, \quad (\text{A.6})$$

$$h^\pm(p)\phi_2^r(q)W_L^{\mp\mu}(r) : \quad \mp \frac{g_w}{2} c_\beta (p-q)_\mu, \quad (\text{A.7})$$

$$h^\pm(p)\phi_2^i(q)W_L^{\mp\mu}(r) : \quad -i \frac{g_w}{2} c_\beta (p-q)_\mu, \quad (\text{A.8})$$

$$G_R^\pm(p)\phi_2^r(q)G_L^\mp(r) : \quad i \frac{g_w}{2M_W} s_\beta M_{\phi_2^r}^2, \quad (\text{A.9})$$

$$G_R^\pm(p)\phi_2^i(q)G_L^\mp(r) : \quad \pm \frac{g_w}{2M_W} s_\beta M_{\phi_2^i}^2, \quad (\text{A.10})$$

$$h^\pm(p)\phi_2^r(q)G_L^\mp(r) : \quad i \frac{g_w}{2M_W} c_\beta (M_h^2 - M_{\phi_2^r}^2), \quad (\text{A.11})$$

$$h^\pm(p)\phi_2^i(q)G_L^\mp(r) : \quad \pm \frac{g_w}{2M_W} s_\beta (M_h^2 - M_{\phi_2^i}^2), \quad (\text{A.12})$$

where s_β is defined in Eq. (2.5) and $\phi_2^{r,i}$ are the FCNC Higgs bosons.

The corresponding couplings of the gauge, Higgs, and would-be Goldstone bosons to the charged leptons and neutrinos can be read off from the Lagrangians:

$$\mathcal{L}_l^{WR} = -\frac{g_w}{\sqrt{2}} W_R^{-\mu} B_{li}^R \bar{l} \gamma_\mu P_R n_i + \text{H.c.}, \quad (\text{A.13})$$

$$\mathcal{L}_l^{GR} = -\frac{g_w}{\sqrt{2}M_W} s_\beta G_R^- B_{li}^R \bar{l} [m_l P_R - m_{n_i} P_L] n_i + \text{H.c.}, \quad (\text{A.14})$$

$$\mathcal{L}_l^{h^-} = \frac{g_w}{\sqrt{2}M_W} c_\beta h^- \bar{l} [B_{li}^R m_l P_R - B_{lj}^R (\delta_{ji} - \frac{C_{ji}^{R*}}{c_\beta^2}) m_{n_j} P_L] n_i + \text{H.c.}, \quad (\text{A.15})$$

$$\begin{aligned}
\mathcal{L}_l^{\phi_2^0} &= -\frac{g_w}{2M_W}\phi_2^r \bar{l}_1 \left[B_{l_{1j}}^L m_{n_j} B_{l_{2j}}^{R*} P_R + B_{l_{1j}}^R m_{n_j} B_{l_{2j}}^{L*} P_L \right] l_2 \\
&\quad -\frac{ig_w}{2M_W}\phi_2^i \bar{l}_1 \left[B_{l_{1j}}^L m_{n_j} B_{l_{2j}}^{R*} P_R - B_{l_{1j}}^R m_{n_j} B_{l_{2j}}^{L*} P_L \right] l_2,
\end{aligned} \tag{A.16}$$

where the mixing matrices B^R and C^R are defined in Section 2, and summation over repeated indices is implied.

Similarly, the interactions of the gauge, Higgs and would-be Goldstone bosons with the quarks may be obtained from the Lagrangians

$$\mathcal{L}_q^{W_R} = -\frac{g_w}{\sqrt{2}} W_R^{+\mu} V_{ij}^{R*} \bar{u}_i \gamma_\mu P_R d_j + \text{H.c.}, \tag{A.17}$$

$$\mathcal{L}_q^{G_R^-} = -\frac{g_w}{\sqrt{2}M_W} s_\beta G_R^+ V_{ij}^{R*} \bar{u}_i \left[m_{d_j} P_L - m_{u_i} P_R \right] d_j + \text{H.c.}, \tag{A.18}$$

$$\mathcal{L}_q^{h^-} = -\frac{g_w}{\sqrt{2}M_W} c_\beta h^- \bar{d}_j \left[V_{ij}^{R*} m_{d_j} P_R - V_{ij}^{R*} m_{u_i} P_L \right] u_i + \text{H.c.}, \tag{A.19}$$

$$\begin{aligned}
\mathcal{L}_q^{\phi_2^0} &= -\frac{g_w}{2M_W}\phi_2^r \bar{d}_2 \left[V_{id_2}^{L*} m_{u_i} V_{id_1}^R P_R + V_{id_2}^{R*} m_{u_i} V_{id_1}^L P_L \right] d_1 \\
&\quad -\frac{ig_w}{2M_W}\phi_2^i \bar{d}_1 \left[V_{id_2}^{L*} m_{u_i} V_{id_1}^R P_R - V_{id_2}^{R*} m_{u_i} V_{id_1}^L P_L \right] l_2,
\end{aligned} \tag{A.20}$$

where V^L and V^R are the corresponding left and right mixing matrices in the quark sector.

B One-loop analytic results

Here, we will present the analytic expressions of all one-loop results. To this end, we first define the following loop functions:

$$\begin{aligned}
I(x, y) &= xy \left\{ -\frac{3}{4} \frac{1}{(1-x)(1-y)} + \left[\frac{1}{4} - \frac{3}{2} \frac{1}{x-1} - \frac{3}{4} \frac{1}{(x-1)^2} \right] \frac{\ln x}{x-y} \right. \\
&\quad \left. + \left[\frac{1}{4} - \frac{3}{2} \frac{1}{y-1} - \frac{3}{4} \frac{1}{(y-1)^2} \right] \frac{\ln y}{y-x} \right\},
\end{aligned} \tag{B.1}$$

$$\begin{aligned}
J_1(x, y, z) &= -\frac{1}{4} \left[\frac{x \ln x}{(x-z)^2(x-y)} + \frac{y \ln y}{(y-z)^2(y-x)} + \frac{1}{(z-x)(z-y)} \right. \\
&\quad \left. + \frac{\ln z}{(z-x)(y-z)} \left(\frac{z}{z-x} - \frac{y}{y-z} \right) \right],
\end{aligned} \tag{B.2}$$

$$\begin{aligned}
J_2(x, y, z) &= \frac{x \ln x}{(1-x)(1-zx)(y-x)} + \frac{y \ln y}{(1-y)(1-zy)(x-y)} \\
&\quad + \frac{z \ln z}{(1-z)(1-zx)(1-zy)},
\end{aligned} \tag{B.3}$$

$$J_3(x, y, z) = \frac{x \ln x}{(x-z)(x-1)(x-y)} + \frac{y \ln y}{(y-z)(y-1)(y-x)}$$

$$+\frac{z \ln z}{(z-1)(z-x)(z-y)}, \quad (\text{B.4})$$

$$F_1(x, y, z) = \frac{x^2 \ln x}{(1-x)(1-zx)(y-x)} + \frac{y^2 \ln y}{(1-y)(1-zy)(x-y)} + \frac{\ln z}{(1-z)(1-zx)(1-zy)}, \quad (\text{B.5})$$

$$F_2(x, y, z) = -\frac{1}{4} \left[\frac{x^2 \ln x}{(x-z)(x-1)(x-y)} + \frac{y^2 \ln y}{(y-z)(y-1)(y-x)} + \frac{z^2 \ln z}{(z-1)(z-x)(z-y)} \right], \quad (\text{B.6})$$

$$E_1(x, y, z, w) = w^2 \left[\frac{x \ln x}{(x-z)(wx-1)(x-y)} + \frac{y \ln y}{(y-z)(wy-1)(y-x)} + \frac{z \ln z}{(wz-1)(z-x)(z-y)} + \frac{w \ln w}{(wz-1)(wx-1)(wy-1)} \right], \quad (\text{B.7})$$

$$E_2(x, y, z, w) = -\frac{w^2}{4} \left[\frac{x^2 \ln x}{(x-z)(wx-1)(x-y)} + \frac{y^2 \ln y}{(y-z)(wy-1)(y-x)} + \frac{z^2 \ln z}{(wz-1)(z-x)(z-y)} + \frac{\ln w}{(wz-1)(wx-1)(wy-1)} \right]. \quad (\text{B.8})$$

Equipped with the above loop functions and the Feynman rules given in Appendix A, we can calculate the individual contribution of the box diagrams, shown in Figs. 2–5, to the decay amplitude of $K_L \rightarrow e\mu$. More explicitly, we have

$$\mathcal{A}(2a) = V_{id}^{L*} V_{is}^L B_{\mu\alpha}^L B_{e\alpha}^{L*} I(\lambda_i, \lambda_\alpha), \quad (\text{B.9})$$

$$\mathcal{A}(2b) = \beta^2 V_{id}^{R*} V_{is}^R B_{\mu\alpha}^R B_{e\alpha}^{R*} I(\beta\lambda_i, \beta\lambda_\alpha), \quad (\text{B.10})$$

$$\mathcal{A}(2c) = V_{id}^{R*} V_{is}^R B_{\mu\gamma}^R B_{e\delta}^{R*} \lambda_i^2 (\lambda_\gamma \lambda_\delta)^{1/2} (s_\beta^2 \delta_{\gamma\alpha} - C_{\gamma\alpha}^L) (s_\beta^2 \delta_{\delta\alpha} - C_{\delta\alpha}^{L*}) J_1(\lambda_i, \lambda_\alpha, \lambda_h), \quad (\text{B.11})$$

$$\mathcal{A}(5a) = V_{id}^{R*} V_{is}^R B_{\mu\gamma}^R B_{e\alpha}^{R*} \lambda_i (\lambda_\alpha \lambda_\gamma)^{1/2} (s_\beta^2 \delta_{\gamma\alpha} - C_{\gamma\alpha}^L) \left[s_\beta^2 E_2(\lambda_i, \lambda_\alpha, \lambda_h, \beta) - E_1(\lambda_i, \lambda_\alpha, \lambda_h, \beta) \right], \quad (\text{B.12})$$

$$\mathcal{A}(5b) = V_{id}^{R*} V_{is}^R B_{\mu\alpha}^R B_{e\gamma}^{R*} \lambda_i (\lambda_\alpha \lambda_\gamma)^{1/2} (s_\beta^2 \delta_{\gamma\alpha} - C_{\gamma\alpha}^{L*}) \left[s_\beta^2 E_2(\lambda_i, \lambda_\alpha, \lambda_h, \beta) - E_1(\lambda_i, \lambda_\alpha, \lambda_h, \beta) \right], \quad (\text{B.13})$$

$$\mathcal{B}(3a) = \beta V_{id}^{L*} V_{is}^R B_{\mu\alpha}^R B_{e\alpha}^{L*} (\lambda_i \lambda_\alpha)^{1/2} \left[\left(1 + \frac{\beta \lambda_i \lambda_\alpha}{4} \right) J_2(\lambda_i, \lambda_\alpha, \beta) - \frac{1+\beta}{4} F_1(\lambda_i, \lambda_\alpha, \beta) \right], \quad (\text{B.14})$$

$$\mathcal{B}(3b) = \beta V_{id}^{R*} V_{is}^L B_{\mu\alpha}^L B_{e\alpha}^{R*} (\lambda_i \lambda_\alpha)^{1/2} \left[\left(1 + \frac{\beta \lambda_i \lambda_\alpha}{4} \right) J_2(\lambda_i, \lambda_\alpha, \beta) - \frac{1+\beta}{4} F_1(\lambda_i, \lambda_\alpha, \beta) \right], \quad (\text{B.15})$$

$$\mathcal{B}(4a) = V_{id}^{L*} V_{is}^R B_{\mu\gamma}^R B_{e\alpha}^{L*} (\lambda_i \lambda_\gamma)^{1/2} (s_\beta^2 \delta_{\gamma\alpha} - C_{\gamma\alpha}^L) \left[F_2(\lambda_i, \lambda_\alpha, \lambda_h) \right]$$

$$-\frac{1}{4}\lambda_i\lambda_\alpha J_3(\lambda_i, \lambda_\alpha, \lambda_h)], \quad (\text{B.16})$$

$$\begin{aligned} \mathcal{B}(4b) = & V_{id}^{R*} V_{is}^L B_{\mu\alpha}^L B_{e\gamma}^{R*} (\lambda_i \lambda_\gamma)^{1/2} (s_\beta^2 \delta_{\gamma\alpha} - C_{\gamma\alpha}^{L*}) [F_2(\lambda_i, \lambda_\alpha, \lambda_h) \\ & - \frac{1}{4}\lambda_i\lambda_\alpha J_3(\lambda_i, \lambda_\alpha, \lambda_h)], \end{aligned} \quad (\text{B.17})$$

where $\beta = M_W^2/M_R^2$, $\lambda_h = M_h^2/M_W^2$, and λ_i and λ_α are defined after Eq. (3.7).

As has been shown in Section 4 however, the sum of the box contributions to \mathcal{B} is not gauge independent by itself. One has to include vertex and self-energy graphs, which are depicted in Figs. 3 and 4. These graphs will restore gauge invariance, after renormalization has been taken into account (see Section 4). Since we are interested in finding the corresponding gauge-dependent complement part of the box contributions to \mathcal{B} in the Feynman-'t Hooft gauge, we keep only those terms that do not vanish in the formal mass limit $M_{\phi_2^{r,i}} \rightarrow \infty$. In Section 4, we have also seen that there will be an implicit dependence of the loop integrals on the FCNC scalar masses, which enters via the OSS renormalization. Furthermore, we take both the FCNC scalars to be exactly degenerate, *i.e.*, $M_{\phi_2^r} = M_{\phi_2^i} = M_\phi$, which is a good approximation (see also Eq. (2.6)). In this way, it is not difficult to find from the would-be Goldstone-boson graphs

$$\begin{aligned} \mathcal{B}(3c + 3d) = & \frac{1}{4} V_{id}^{L*} V_{is}^R B_{\mu\alpha}^R B_{e\alpha}^{L*} s_\beta^2 \lambda_i^{3/2} \lambda_\alpha^{1/2} C_0^{R1}(0, \lambda_\phi, 0, \lambda_i, 1, 1/\beta) \\ & + \frac{1}{4} V_{id}^{R*} V_{is}^L B_{\mu\alpha}^L B_{e\alpha}^{R*} s_\beta^2 \lambda_i^{3/2} \lambda_\alpha^{1/2} C_0^{R1}(0, \lambda_\phi, 0, \lambda_i, 1, 1/\beta), \end{aligned} \quad (\text{B.18})$$

$$\begin{aligned} \mathcal{B}(3e + 3f) = & \frac{1}{4} V_{id}^{L*} V_{is}^R B_{\mu\alpha}^R B_{e\alpha}^{L*} s_\beta^2 \lambda_i^{1/2} \lambda_\alpha^{3/2} C_0^{R1}(0, \lambda_\phi, 0, \lambda_\alpha, 1, 1/\beta) \\ & + \frac{1}{4} V_{id}^{R*} V_{is}^L B_{\mu\alpha}^L B_{e\alpha}^{R*} s_\beta^2 \lambda_i^{1/2} \lambda_\alpha^{3/2} C_0^{R1}(0, \lambda_\phi, 0, \lambda_\alpha, 1, 1/\beta), \end{aligned} \quad (\text{B.19})$$

$$\begin{aligned} \mathcal{B}(3g + 3h) = & \frac{1}{16} V_{id}^{L*} V_{is}^R B_{\mu\alpha}^R B_{e\alpha}^{L*} \beta (\lambda_i \lambda_\alpha)^{1/2} B_0^{R2}(\lambda_\phi, 1, 1/\beta) \\ & + \frac{1}{16} V_{id}^{R*} V_{is}^L B_{\mu\alpha}^L B_{e\alpha}^{R*} \beta (\lambda_i \lambda_\alpha)^{1/2} B_0^{R2}(\lambda_\phi, 1, 1/\beta), \end{aligned} \quad (\text{B.20})$$

$$\begin{aligned} \mathcal{B}(4c + 4d) = & \frac{1}{4} (1 - \lambda_h/\lambda_\phi) V_{id}^{L*} V_{is}^R B_{\mu\alpha}^R B_{e\alpha}^{L*} c_\beta^2 \lambda_i^{3/2} \lambda_\alpha^{1/2} C_0^{R1}(0, \lambda_\phi, 0, \lambda_i, 1, \lambda_h) \\ & + \frac{1}{4} (1 - \lambda_h/\lambda_\phi) V_{id}^{R*} V_{is}^L B_{\mu\alpha}^L B_{e\alpha}^{R*} s_\beta^2 \lambda_i^{3/2} \lambda_\alpha^{1/2} C_0^{R1}(0, \lambda_\phi, 0, \lambda_i, 1, \lambda_h), \end{aligned} \quad (\text{B.21})$$

$$\begin{aligned} \mathcal{B}(4e + 4f) = & \frac{1}{4} (1 - \lambda_h/\lambda_\phi) V_{id}^{L*} V_{is}^R B_{\mu\gamma}^R B_{e\alpha}^{L*} (s_\beta^2 \delta_{\alpha\gamma} - C_{\alpha\gamma}^L) \lambda_i^{1/2} \lambda_\alpha \lambda_\gamma^{1/2} \\ & \times C_0^{R1}(0, \lambda_\phi, 0, \lambda_\alpha, 1, \lambda_h) + \frac{1}{4} (1 - \lambda_h/\lambda_\phi) V_{id}^{R*} V_{is}^L B_{\mu\alpha}^L B_{e\gamma}^{R*} \\ & \times (s_\beta^2 \delta_{\alpha\gamma} - C_{\alpha\gamma}^{L*}) \lambda_i^{1/2} \lambda_\gamma^{1/2} \lambda_\alpha C_0^{R1}(0, \lambda_\phi, 0, \lambda_\alpha, 1, \lambda_h), \end{aligned} \quad (\text{B.22})$$

$$\mathcal{B}(4g + 4h) = \frac{1}{16} (1 - \lambda_h/\lambda_\phi)^2 V_{id}^{L*} V_{is}^R B_{\mu\alpha}^R B_{e\alpha}^{L*} c_\beta^2 (\lambda_i \lambda_\alpha)^{1/2} B_0^{R2}(\lambda_\phi, 1, \lambda_h)$$

$$+\frac{1}{16}(1-\lambda_h/\lambda_\phi)^2 V_{id}^{R*} V_{is}^L B_{\mu\alpha}^L B_{e\alpha}^{R*} \beta(\lambda_i \lambda_\alpha)^{1/2} B_0^{R2}(\lambda_\phi, 1, \lambda_h). \quad (\text{B.23})$$

Since $\lambda_h - \lambda_\phi = \mathcal{O}(1)$, as has been discussed in Section 2, the reduced amplitudes $\mathcal{B}(4c+4d)$, $\mathcal{B}(4e+4f)$ and $\mathcal{B}(4g+4h)$ behave as $1/\lambda_\phi$ and $1/\lambda_\phi^2$. Therefore, these contributions may safely be neglected in the numerical estimates.

The OSS renormalization scheme adopted in Section 4 gives rise to the subtracted loop functions C_0^{R1} and B_0^{R2} , which are defined in the following way:

$$B_0^{R2}(M^2, m_1^2, m_2^2) = B_0(0, m_1^2, m_2^2) - B_0(M^2, m_1^2, m_2^2) + M^2 B_0'(M^2, m_1^2, m_2^2), \quad (\text{B.24})$$

$$C_0^{R1}(0, M^2, 0, m_1^2, m_2^2, m_3^2) = C_0(0, 0, 0, m_1^2, m_2^2, m_3^2) - C_0(0, M^2, 0, m_1^2, m_2^2, m_3^2). \quad (\text{B.25})$$

The loop functions $B_0(M^2, m_1^2, m_2^2)$ and $C_0(0, M^2, 0, m_1^2, m_2^2, m_3^2)$ are the usual Passarino-Veltman functions defined in Ref. [37]. Their explicit form is given by

$$B_0(M^2, m_1^2, m_2^2) = C_{\text{UV}} - \ln(m_1 m_2) + 2 + \frac{1}{M^2} \left[(m_2^2 - m_1^2) \ln \frac{m_1}{m_2} + \lambda^{1/2}(M^2, m_1^2, m_2^2) \cosh^{-1} \left(\frac{m_1^2 + m_2^2 - M^2}{2m_1 m_2} \right) \right], \quad (\text{B.26})$$

$$C_0(0, M^2, 0, m_1^2, m_2^2, m_3^2) = -\frac{1}{M^2} \left[\text{Li}_2 \left(\frac{m_1^2 - m_3^2}{m_1^2 - m_3^2 + M^2 \xi_+} \right) - \text{Li}_2 \left(\frac{m_1^2 - m_3^2 + M^2}{m_1^2 - m_3^2 + M^2 \xi_+} \right) + \text{Li}_2 \left(\frac{m_1^2 - m_3^2}{m_1^2 - m_3^2 + M^2 \xi_-} \right) - \text{Li}_2 \left(\frac{m_1^2 - m_3^2 + M^2}{m_1^2 - m_3^2 + M^2 \xi_-} \right) - \text{Li}_2 \left(\frac{(m_1^2 - m_2^2)(m_1^2 - m_3^2)}{(m_1^2 - m_2^2)(m_1^2 - m_3^2) + M^2 m_1^2} \right) + \text{Li}_2 \left(\frac{(m_1^2 - m_2^2)(m_1^2 - m_3^2 + M^2)}{(m_1^2 - m_2^2)(m_1^2 - m_3^2) + M^2 m_1^2} \right) \right], \quad (\text{B.27})$$

where $\lambda(x, y, z) = (x - y - z)^2 - 4yz$, $\cosh^{-1} z = \ln(z + \sqrt{z^2 - 1})$ and C_{UV} is an UV constant which drops out after renormalization. Furthermore, in Eq. (B.27), we have defined

$$\xi_\pm = \frac{1}{2M^2} [M^2 - m_2^2 + m_3^2 \pm \lambda^{1/2}(M^2, m_2^2, m_3^2)], \quad (\text{B.28})$$

and the dilogarithmic function

$$\text{Li}_2(x \pm i\varepsilon) = -\int_0^x dt \frac{\ln|1-t|}{t} \pm i\theta(x-1)\pi \ln x. \quad (\text{B.29})$$

References

- [1] Particle Data Group, R.M. Barnett *et al.*, Phys. Rev. **D54** (1996) 1.
- [2] For reviews on $K^0\bar{K}^0$ mixing and CP violation, see, E.A. Paschos and U. Türke, Phys. Rep. **178** (1989) 145; W. Grimus, Fortschr. Phys. **36** (1988) 201; R. Decker, Fortschr. Phys. **37** (1989) 657; P.K. Kabir, “The CP puzzle,” Academic Press, London and New York, 1968; B. Winstein and L. Wolfenstein, Rev. Mod. Phys. **65** (1993) 1113.
- [3] E. Eichten, I. Hinchliffe, K.D. Lane and C. Quigg, Phys. Rev. **D34** (1986) 1547; J.C. Pati and H. Stremnitzer, Phys. Lett. **B172** (1986) 441; I. Bigi, G. Köpp and P.M. Zerwas, Phys. Lett. **B166** (1986) 238.
- [4] B.A. Campbell, Phys. Rev. **D28** (1983) 209; B.A. Campbell, J. Ellis, K. Enqvist, M.K. Gaillard and D.V. Nanopoulos, Int. J. Mod. Phys. **A2** (1987) 831.
- [5] W.-S. Hou and A. Soni, Phys. Rev. Lett. **54** (1985) 2038.
- [6] O. Shanker, Nucl. Phys. **B206** (1982) 253; L.J. Hall and L.J. Randall, Nucl. Phys. **B274** (1986) 157.
- [7] T. Inami and C.S. Lim, Prog. Theor. Phys. **65** (1981) 297; 1772 (Errata).
- [8] C.S. Lim and T. Inami, Prog. Theor. Phys. **67** (1982) 1569.
- [9] P. Langacker, S.U. Sankar and K. Schilcher, Phys. Rev. **D38** (1988) 2841.
- [10] Z. Gagyi-Palfy, A. Pilaftsis and K. Schilcher, Phys. Lett. **B343** (1995) 275.
- [11] R.N. Mohapatra and G. Senjanović, Phys. Rev. **D23** (1981) 165.
- [12] T. Yanagida, Proceedings of the *Workshop on Unified Theory and Baryon Number of the Universe*, eds. O. Swada and A. Sugamoto (KEK, 1979) p. 95; M. Gell-Mann, P. Ramond, and R. Slansky, *Supergravity*, eds. P. van Nieuwenhuizen and D. Friedman (North-Holland, Amsterdam, 1979) p. 315; R.N. Mohapatra and G. Senjanović, Phys. Rev. Lett. **44** (1980) 912.
- [13] A. Pilaftsis, Phys. Lett. **B285** (1992) 68; Mod. Phys. Lett. **A9** (1994) 3595.
- [14] A. Ilakovac and A. Pilaftsis, Nucl. Phys. **B437** (1995) 491.
- [15] J.G. Körner, A. Pilaftsis and K. Schilcher, Phys. Lett. **B300** (1993) 381.

- [16] J. Bernabéu, J.G. Körner, A. Pilaftsis and K. Schilcher, Phys. Rev. Lett. **71** (1993) 2695; J. Bernabéu and A. Pilaftsis, Phys. Lett. **B351** (1995) 235.
- [17] A. Pilaftsis, Phys. Rev. **D52** (1995) 459.
- [18] W.-S. Hou and A. Soni, Phys. Rev. **D32** (1985) 163.
- [19] J. Basecq, L.F. Li and P.B. Pal, Phys. Rev. **D32** (1985) 175.
- [20] J.C. Pati and A. Salam, Phys. Rev. **D10** (1974) 275.
- [21] H. Fritzsch and P. Minkowski, Ann. Phys. **93** (1975) 193.
- [22] J.F. Gunion, J. Grifols, A. Mendez, B. Kayser, and F. Olness, Phys. Rev. **D40** (1989) 1546.
- [23] G. Senjanović, Nucl. Phys. **B153** (1979) 334.
- [24] D. Chang and R.N. Mohapatra, Phys. Rev. **D32** (1985) 1248.
- [25] A. Pilaftsis, Phys. Rev. **D49** (1994) 2398.
- [26] A. Pilaftsis, Z. Phys. **C55** (1992) 275.
- [27] P. Langacker and D. London, Phys. Rev. **D38** (1988) 886; G. Bhattacharyya, A. Datta, S.N. Ganguli, and A. Raychaudhuri, Mod. Phys. Lett. **A6** (1991) 2921.
- [28] D. Wyler and L. Wolfenstein, Nucl. Phys. **B218** (1983) 205.
- [29] B.A. Kniehl and A. Pilaftsis, Nucl. Phys. **B474** (1996) 286.
- [30] J.D. Vergados, Phys. Rep. **133** (1986) 1.
- [31] J. Gasser and H. Leutwyler, Phys. Rep. **87** (1982) 77.
- [32] M.E. Pospelov, Phys. Rev. **D56** (1997) 259.
- [33] F.I. Olness and M.E. Ebel, Phys. Rev. **D32** (1985) 1769.
- [34] For example, see, K.-I. Aoki, Z. Hioki, R. Kawabe, M. Konuma and T. Muta, Prog. Theor. Phys. Suppl. **73** (1982) 1; M. Böhm, H. Spiesberger and W. Hollik, Fortschr. Phys. **34** (1986) 687.
- [35] G. Ecker and W. Grimus, Nucl. Phys. **B258** (1985) 328.
- [36] G. Barenboim, J. Bernabéu and M. Raidal, Nucl. Phys. **B478** (1996) 527.

- [37] G. 't Hooft and M. Veltman, Nucl. Phys. **B153** (1979) 365; G. Passarino and M. Veltman, Nucl. Phys. **B160** (1979) 151.

Figures 7 – 12

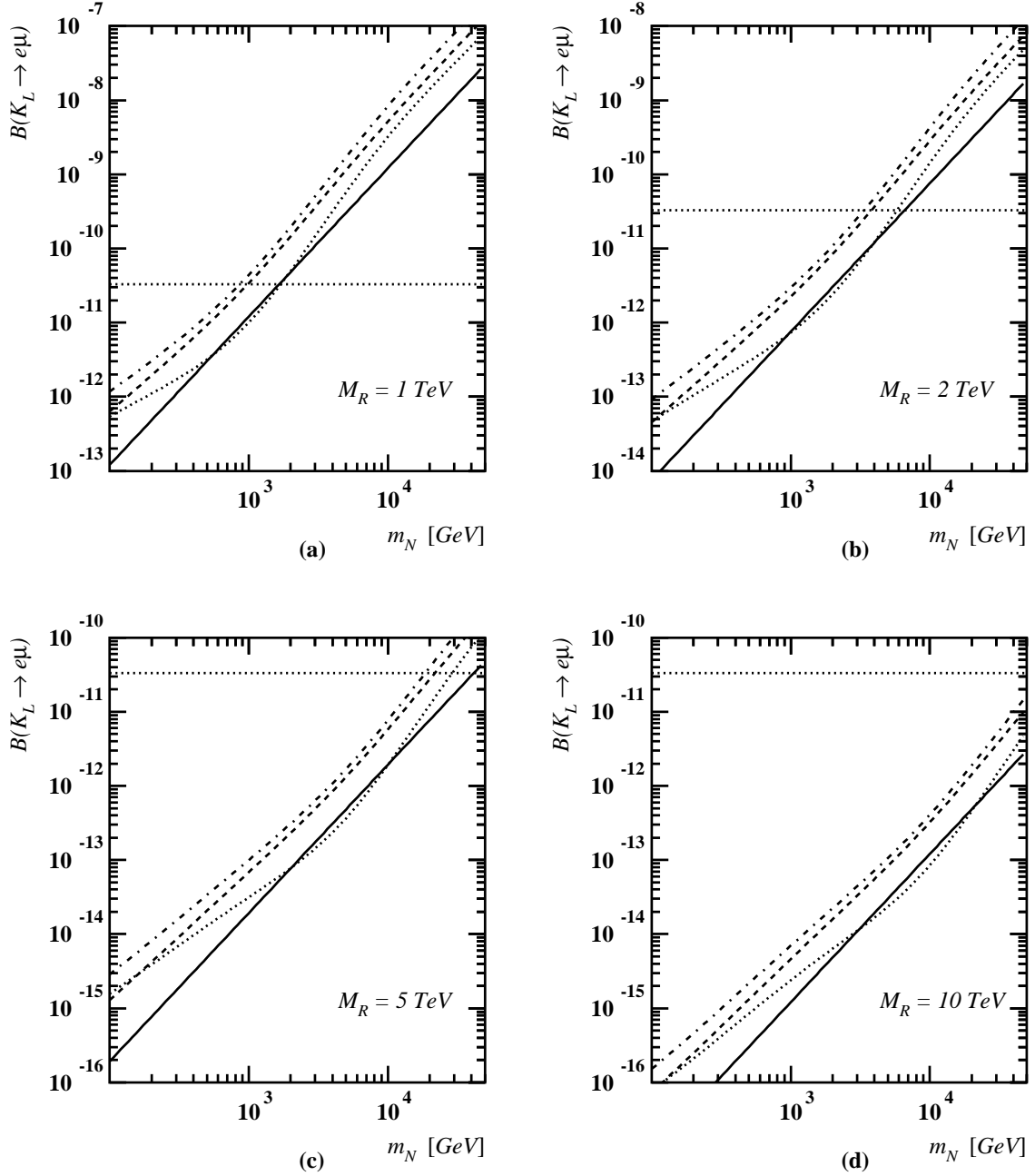


Fig. 7: $B(K_L \rightarrow e\mu)$ versus m_N for different M_R values in the manifest LRSM (the meaning of the various lines is given in the text).

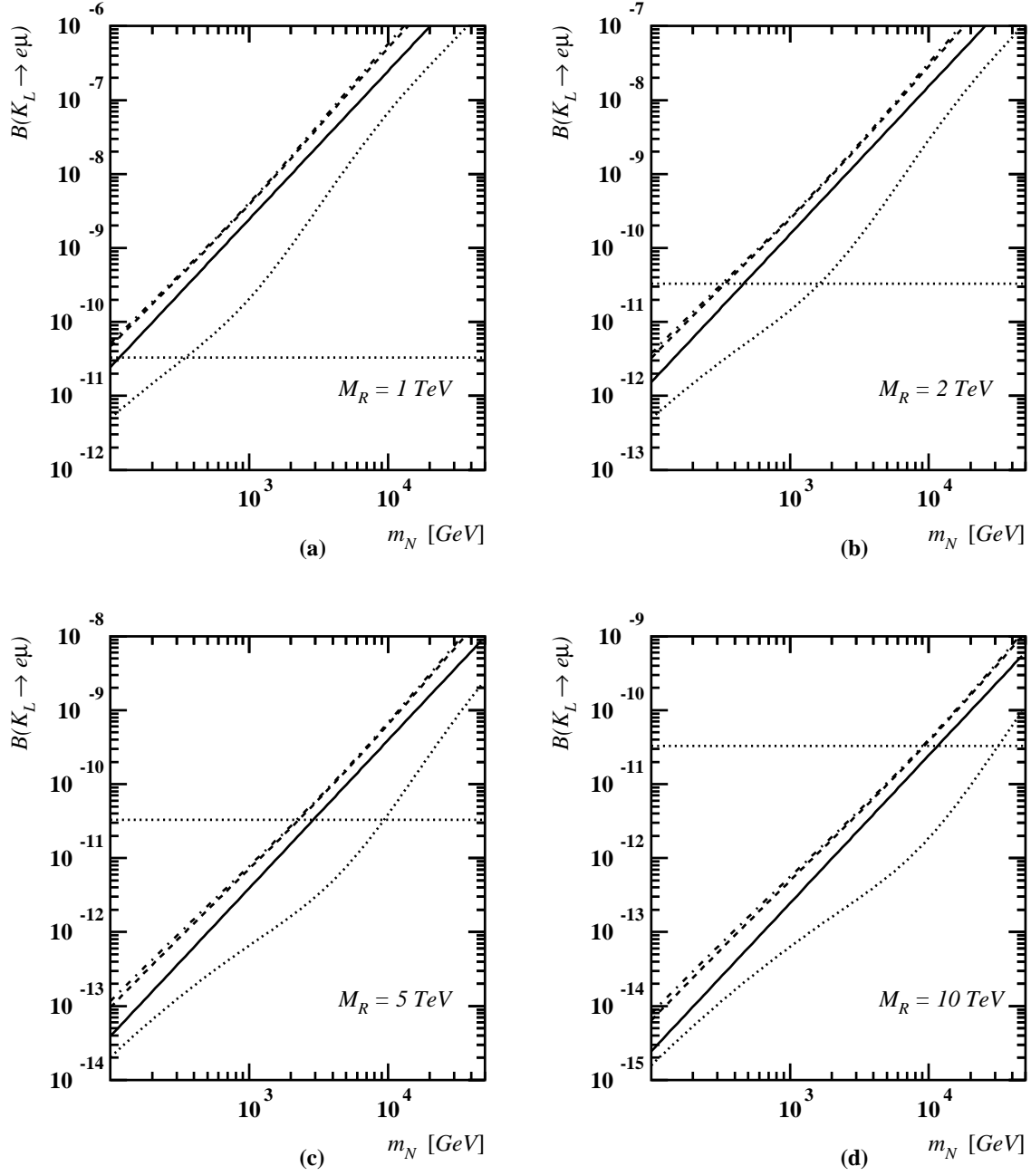


Fig. 8: $B(K_L \rightarrow e\mu)$ versus m_N for different M_R values in the non-manifest LRSM (the meaning of the various lines is given in the text).

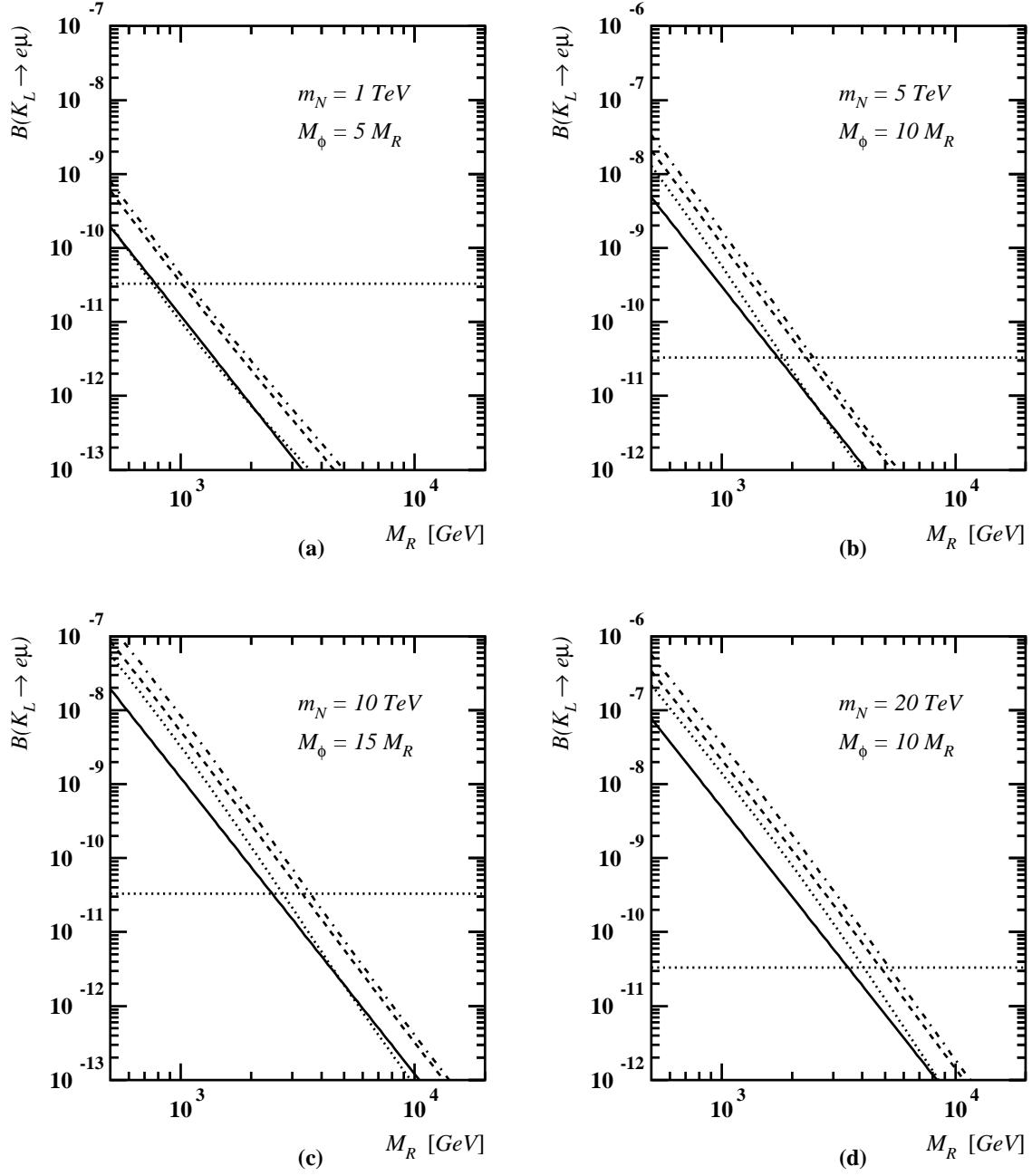


Fig. 9: $B(K_L \rightarrow e\mu)$ versus M_R for different m_N values in the manifest LRSM (the meaning of the various lines is given in the text).

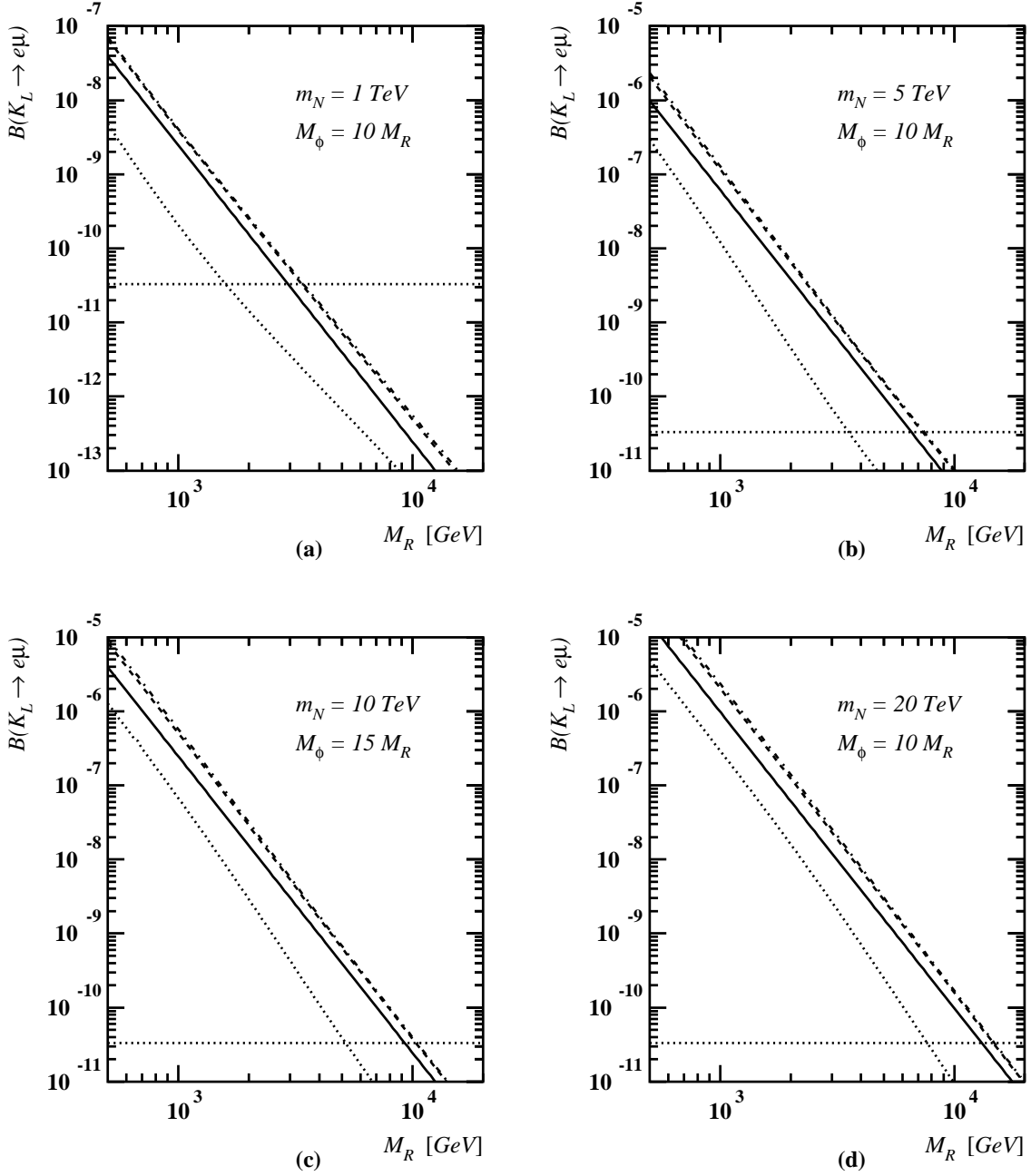


Fig. 10: $B(K_L \rightarrow e\mu)$ versus M_R for different m_N values in the non-manifest LRSM (the meaning of the various lines is given in the text).

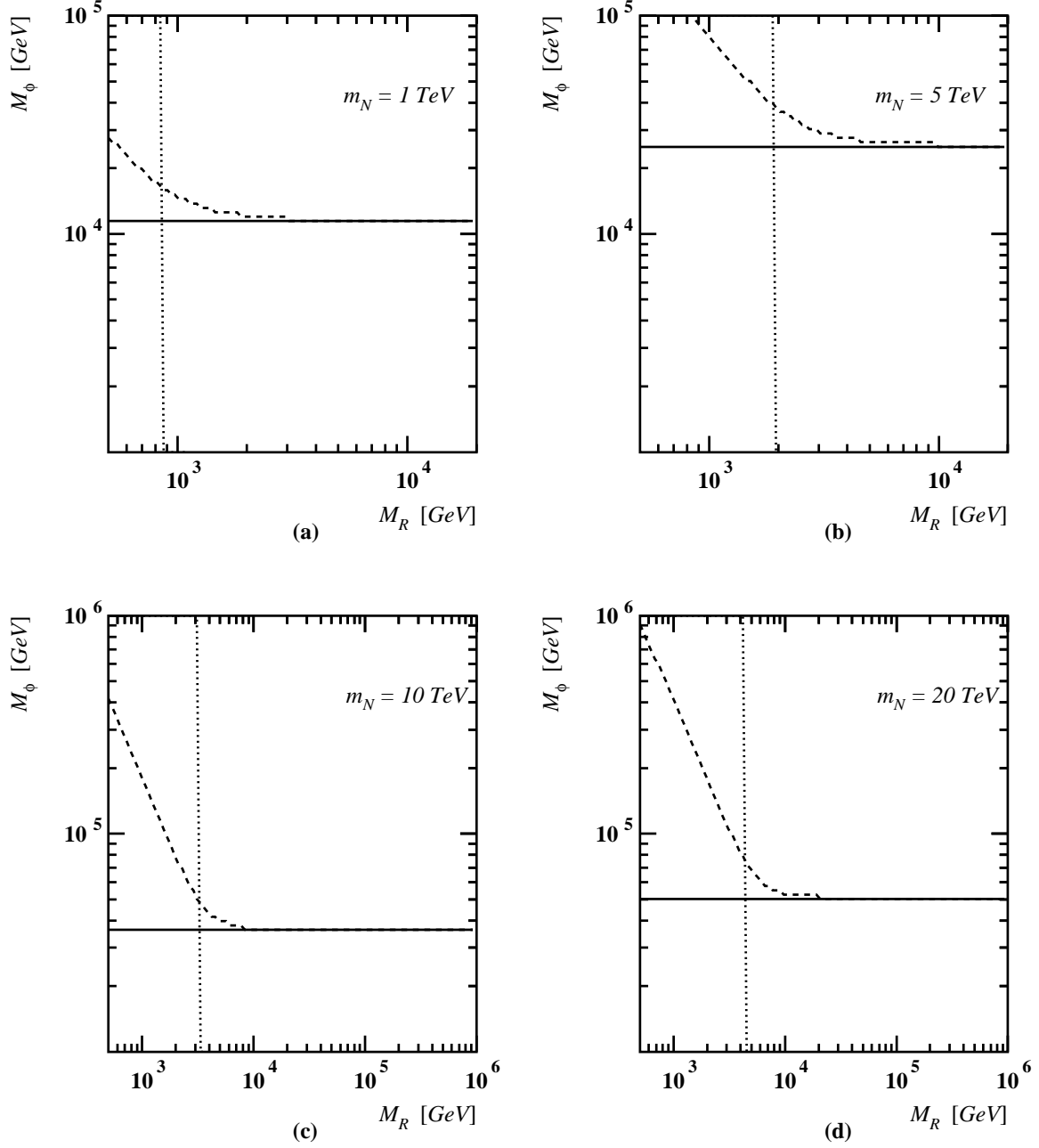


Fig. 11: Exclusion plots for the parameters M_ϕ , M_R , obtained from the constraint $B(K_L \rightarrow e\mu) < 3.3 \times 10^{-11}$ in the manifest LRSM (the meaning of the various lines is given in the text).

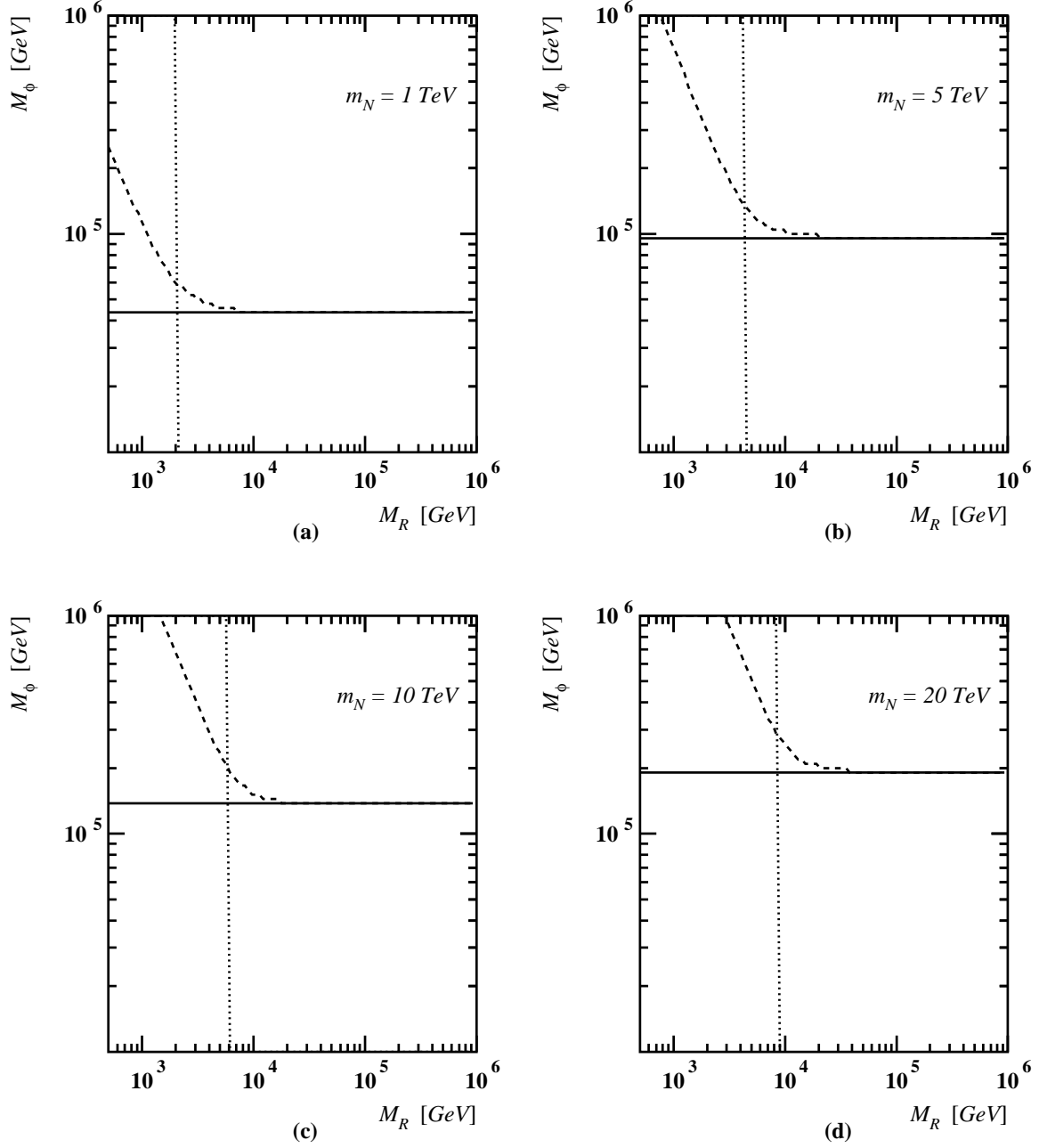


Fig. 12: Exclusion plots for the parameters M_ϕ , M_R , obtained from the constraint $B(K_L \rightarrow e\mu) < 3.3 \times 10^{-11}$ in the non-manifest LRSM (the meaning of the various lines is given in the text).